

# Adaptive Gaussian Process based Stochastic Trajectory Optimization for Motion Planning

Feng Yichang, Zhang Haiyun, Wang Jin, and Lu Guodong,

**Abstract**—We propose a new formulation of optimal motion planning (OMP) algorithm for robots operating in a hazardous environment, called adaptive Gaussian-process based stochastic trajectory optimization (AGP-STO). It first restarts the accelerated gradient descent with the reestimated Lipschitz constant ( $\mathcal{L}$ -reAGD) to improve the computation efficiency, only requiring 1st-order momentum. However, it still cannot infer a global optimum of the nonconvex problem, informed by the prior information of Gaussian-process (GP) and obstacles. So it then integrates the adaptive stochastic trajectory optimization (ASTO) in the  $\mathcal{L}$ -reestimation process to learn the GP-prior rewarded by the important samples via accelerated moving averaging (AMA). Moreover, we introduce the incremental optimal motion planning (iOMP) to upgrade AGP-STO to iAGP-STO. It interpolates the trajectory incrementally among the previously optimized waypoints to ensure time-continuous safety. Finally, we benchmark iAGP-STO against the numerical (CHOMP, TrajOpt, GPMP) and sampling (STOMP, RRT-Connect) methods and conduct the tuning experiment of key parameters to show how the integration of  $\mathcal{L}$ -reAGD, ASTO, and iOMP elevates computation efficiency and reliability. Moreover, the implementation of iAGP-STO on LBR-iiwa, multi-AGV, and rethink-Baxter demonstrates its application in manipulation, collaboration, and assistance.

## I. INTRODUCTION

Industrial robot plays a vital role in manufactory benefited from their high flexibility, efficiency, and robustness compared to manual labor in some repetitive works. However, most robotization achieves via manual programming or teaching. It is time-consuming to assign every support waypoint motion, resulting in low flexibility and adaptation facing the space or time-varying of the working condition. Motion planning is crucial for robots to safely execute complex tasks in a harsh workspace (W-space).

Optimal motion planning (OMP), a.k.a. trajectory optimization, tends to find a series of collision-free waypoints satisfying the task requirements. Some former studies search for an optimal solution via numerical optimization [1]–[3] or probabilistic sampling [4]–[7] in configuration space (C-space) or W-space. The numerical method can rapidly approach minima by serial descent steps and adapt to a dynamic environment, while the minima’s feasibility highly depends on the initial point. The sampling-based method can overcome this problem regardless of the high computational cost of high-dimensional searching space with narrow feasible subspace.

(i) Though some numerical methods [2], [3] adopt the trust-region or line search methods for solution search, the trust-

region adjustment or quasi-Hessian matrix estimation will consume the extra computation resource and finally approach the local minimum.

(ii) The graph searching methods [5], [6], [8] construct a probabilistic roadmap in C-space with random vertex sampling and shortest branch connection. However, they require massive computational resources for repeated collision-check and roadmap storage. The trajectory sampling methods [1], [7] flatten this issue via resampling a limited number of noisy trajectories regardless of the lower success rate.

(iii) Though some fusion methods [1], [9], [10] integrate the numerical and probabilistic methods for path smoothing and success rate improvement, the limited searching process restrains the environmental information gathering for OMP.

To solve the above concerns, iAGP-STO makes an incremental probabilistic inference of an optimal trajectory based on the adaptive Gaussian process (AGP), integrating stochastic learning and numerical trajectory optimization (STO).

(i) Considering the high convexity requirement [2] and the extra computation resource [3], AGP-STO adopts accelerated gradient descent (AGD) [11] and restarts it with the reestimated Lipschitz constant ( $\mathcal{L}$ -reAGD). It also adopts the penalty method [12] to gather the GP prior and obstacle information to maximize a posterior. To elevate the efficiency further, we incrementally optimize the motion planning (iOMP) by constructing a Bayes tree consisting of factors informed by GP prior, obstacle, and other motion constraints and optimize the sub-trajectories containing significant factors.

(ii) Like other numerical methods,  $\mathcal{L}$ -reAGD easily encounters the local minima when a dense obstruction is in the W-space. Therefore, we judge whether a minimum approaches during  $\mathcal{L}$ -reestimation. When it approaches, adaptive stochastic trajectory optimization (ASTO) will resample noise trajectories, gain the reward via expectation-maximization and learn the GP-policy via accelerated moving averaging (AMA) to infer a trajectory located in a convex subspace.

(iii) Unlike CHOMP [1] alternating between resampling and leapfrog, AGP-STO inserts the ASTO in the  $\mathcal{L}$ -reestimation depending on whether a minimum exists and then infers an optimal policy learned from ASTO via  $\mathcal{L}$ -reAGD until convergence. Besides, it utilizes  $\mathcal{L}$ -reAGD to restrain the searching space of ASTO, unlike CBiRRT [9], reducing the C-space dimension by finding the null-space of constraints.

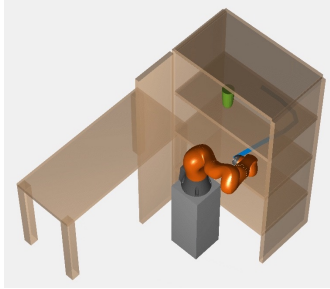
Finally, we have successfully implemented iAGP-STO on LBR-iiwa (Figure 1) in 25 tasks with different initial and goal states. All tasks are categorized into three classes (A, B, C) to benchmark iAGP-STO against  $\mathcal{L}$ -reAGD, AGP-STO, and other

Wang Jin, corresponding author, State Key Laboratory of Fluid Power and Mechatronic Systems, School of Mechanical Engineering, Zhejiang University, Hangzhou, Zhejiang, China. dwjcom@zju.edu.cn

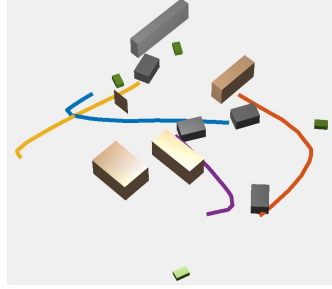
Manuscript received Xxx xx, 20xx; revised Xxx xx, 20xx.

TABLE I: Terms of Abbreviation

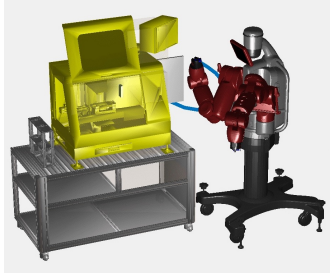
| abbr.                      | meaning  | abbr.    | meaning                      |
|----------------------------|--|----------|------------------------------|
| AGP-STO                    | adaptive gaussian process based stochastic trajectory optimization | iAGP-STO | incremental AGP-STO          |
| AGD   $\mathcal{L}$ -reAGD | accelerated gradient descent   Lipschitz restarted AGD             | HMC      | Hamiltonian Monte-carlo      |
| ASTO                       | adaptive stochastic trajectory optimization                        | AMA      | accelerated moving averaging |
| GP   $\mathcal{GP}$        | Gaussian process   GP distribution or model                        | CCB      | collision-check box or ball  |
| BT   BTI                   | Bayes tree   BT inference  | MAP      | maximize a posterior         |
| W- C- T-space              | work configuration trajectory -space                               | OMP      | optimal motion planning      |



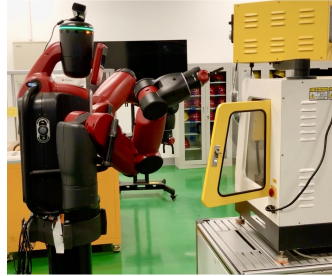
(a) LBR-iiwa manipulates in a shelf.



(b) 4 AGVs collaborate in a warehouse.



(c) rethink-Baxter assists at a machine.



(d) The real experiment of rethink-Baxter.

Fig. 1: Different problems of optimal motion planning (OMP).

algorithms, such as CHOMP [1], GPMP [3], TrajOpt [13], STOMP [7] and RRT-Connect [5]. The benchmark results show that AGP-STO has an eminently higher success rate, especially in the Class C task. However, it takes more time for iAGP-STO to generate the trajectory than the numerical methods. Besides, the results of tuning and cross-validation experiments show how  $\mathcal{L}$ -reAGD, ASTO, and iOMP unite to achieve highly reliable and efficient planning. Furthermore, we conduct the simulation experiments on a multi-AGV system and the real experiments on a single arm of rethink-Baxter, as shown in Figure 1. Table I provides the terms of abbreviation.

## II. RELATED WORKS

### A. Formulation of Optimal Motion Planning

Since OMP optimizes the objective functional meeting the motion constraints to gain an optimal trajectory, it is essential to formulate the constrained optimization problem (COP). Recent studies can be divided into whole trajectory optimization and local waypoints adaptation.

1) *Whole Trajectory Optimization*: The former studies of whole trajectory optimization, such as CHOMP [1], ITOMP [14], TrajOpt (a.k.a. SCO) [2], [13] and GPMP [3], all adopt an objective functional consisting of smooth term

and obstacle constrained terms. In the smooth term, CHOMP, ITOMP, and TrajOpt adopt the kinetic energy form, while GPMP uses the GP model. As for the obstacle term, all of them except for TrajOpt employ the body-obstacle kinetic energy [1], [15], [16]. TrajOpt uses a fixed convex combination of constraint gradients in adjacent time to ensure the time-continuous safety, while GPMP uses an up-sampling method. Moreover, the penalty factor [12] is adopted to optimize the objective under collision-free constraints. Most of the recent studies [1], [3] transform the SDF [17] into a non-negative obstacle cost function and use constant trade-off parameter, while TrajOpt uses the  $\ell_1$ -penalty method [12].

2) *Local Waypoints Adaptation*: As for the local waypoints adaptation method, ITOMP [14] interleaves of planning and execution using the prediction of environment change for real-time replanning. The algorithmic safety measure [18] uses the model-predictive control and proposes a time continuously differentiable obstacle cost function for real-time collision avoidance. GPMP2 [19] adopts iSAM2 [20] and applies BTI [21] for sparse nonlinear incremental optimization. Note that a wide range of recent studies has applied Bayes inference in simultaneous localization and mapping [22], [23], pattern recognition [24], [25] and OMP [3], [19], [26] for the convenience to apply quasi-Newton method.

### B. Numerical Optimization

As the main branch of OMP study, numerical optimization searches for the optimum on the manifold of COP in the trajectory space. Its studies could be divided into Quasi-Newton, gradient descent, and stochastic optimization method according to the estimation method of descent step.

1) *Quasi-Newton Method*: The Newton method [12] solves linear systems to achieve a superlinear convergence. However, it consumes numerous resources for a Hessian matrix and its inverse. So the quasi-Newton method always approximates Hessian via LM [19], [27], [28], BFGS [29], [30] et al. to gain the same rate. GPMP2 [3] recently adopts the LM method to solve the MAP problem given the prior information. Besides, machining learning and OMP [31] apply the limited-memory BFGS (L-BFGS) [32] and damped BFGS (dBFGS) [33] algorithm for high dimensional optimization and optimal control, respectively. Because L-BFGS and dBFGS only require 1st order information for superlinear convergence.

2) *Gradient Descent Method*: In contrast to the Newton or quasi-Newton method, gradient descent needs to estimate the step size rather than Hessian. It contains two main methods: the line search [34] and the trust-region method [35], [36]. In practice, CHOMP [1] and GPMP [3] both use a fixed step, while TrajOpt [13] adopts the trust region method.

3) *Stochastic Optimization*: Unlike the exact numerical optimization method, the stochastic gradient descent (SGD) [37] methods, such as Adam [38], RMSProp [39], and Ada-Grad [40], always program the object composed of a sum of weakly coupling sub-functions and generates the sub-gradients via the random selections of sub-functions. Our recent work [41] proposes iSAGO based on SGD to overcome the local minima brought by the body-obstacle stuck case. During SGD, they all adopt Nesterov's accelerated gradient descent (AGD) [11], [42], which forms a projection from a current step into its near future. Moreover, the AGD steps, containing the stochastic gradients, optimize machine learning progress [43]–[45], whose convergence rate correlates with the order of the Lipschitz constant.

### C. Probabilistic Sampling

The sampling-based method samples waypoints or trajectories dynamically in the configuration space (C-space) or working space (W-space).

1) *Roadmap Construction*: Though A\* [46] introduces a heuristic function for the forward cost estimation, its dynamic programming takes numerous computation resources for OMP. Rapid random tree (RRT) [4] treats OMP as a tree search problem to solve this concern. As an upgrade of RRT, RRT\* [6] appends the original construction of RRT with a rewiring process to shorten the path. RRT-connect [5] introduces the bidirectional searching method to improve efficiency. The law of the above algorithms is abstracted by the random nearest-neighbor-type graph [47]. LQR-RRT\* [48] combines RRT\* with the linear-quadratic regulator for optimal manipulation control. Unlike RRT methods, PRMs [8], [49], [50] randomly generate and connect numerous collision-free configurations to construct a probabilistic road map. However, the generation of several collision-free waypoints always consumes more time with less optimality than RRT and RRT\*. FFRob [51] introduces extended action specifications to make a general representation of planning problems and adopts RRT-connect and sPRM to construct a conditional reachability graph.

2) *Trajectory Sampling*: Despite the above sampling methods, STOMP [7] adopts the objective functional form of [1] and optimizes the trajectory via noise trajectory resampling obeying Gaussian distribution renewed by the selected samplings. [52] introduces the GP model into the stochastic process of STOMP to improve the searching efficiency. Recently, SMTO [53] upgraded STOMP's sampling model by applying Monte-Carlo optimization for multi-solution solving and using the numerical method for policy refinement.

## III. BACKGROUND

### A. Accelerated Gradient Descent

Nesterov's AGD [42] makes faster nonlinear programming than gradient descent [34] yet takes more steps than the quasi-Newton method [54], benefiting from Hessian estimation. This none Hessian method performs efficiently [55] in some high-dimensional, even nonconvex problems. Section VI adopts AGD for GP inference of trajectory given the obstacle

information, while Section VII adopts it for adaptive GP-learning during the trajectory resampling. For generalization, this section abstracts them as

$$\arg \min_{\mathbf{x} \in \mathbb{R}^n} \Psi(\mathbf{x}) \quad (1)$$

and assumes

$$\|\nabla \Psi(\mathbf{y}) - \nabla \Psi(\mathbf{x})\| \leq \mathcal{L}_\Psi \|\mathbf{y} - \mathbf{x}\| \quad \forall \mathbf{x}, \mathbf{y} \in \mathcal{X}, \quad (2)$$

where  $\mathcal{X} \subseteq \mathbb{R}^n$  is a locally convex subspace with Lipschitz ( $\mathcal{L}_\Psi$ ) continuous gradient  $\nabla \Psi$ .

**Lemma 1.** *Let  $\{\alpha_k\}$  be a series of forgetting coefficients, each of whom selects a point between  $\mathbf{x}^{ag}$  and  $\mathbf{x}$ , and  $\gamma_k$  be a sequence satisfying*

$$\gamma_k \leq (1 - \alpha_k) \gamma_{k-1} + \eta_k, \quad k = 1, 2, \dots, N$$

where we define another sequence

$$\Gamma_k := \begin{cases} 1, & k = 1 \\ (1 - \alpha_k) \Gamma_{k-1}, & k \geq 2. \end{cases} \quad (3)$$

Then we have

$$\gamma_k \leq \Gamma_k \sum_{i=1}^k (\eta_i / \Gamma_i), \quad \forall k > 1.$$

Unlike the traditional methods [34], [56] performing steepest descent in each step, Ghadimi's AGD [11] introduces  $\lambda_k$  to release the primary steps from steepest descent and  $\beta_k$  to ensure a robust convergence in some nonconvex cases.

---

#### Algorithm 1: AGD

---

**Input** : initial  $\mathbf{x}_0$ , objective function  $\Psi$ , Lipschitz constant  $\mathcal{L}_\Psi$ , update rule  $\{\alpha_k, \beta_k, \lambda_k\}$ , and termination condition  $\text{AccBreak}()$ .

```

1 Initialize:  $\{\mathbf{x}_0^{md}, \mathbf{x}_0^{ag}\} \leftarrow \mathbf{x}_0$ ;
2 for  $\text{AgdIter} : k = 1 \dots N_{ag}$  do
3    $\mathbf{x}_k^{md} = (1 - \alpha_k) \mathbf{x}_{k-1}^{ag} + \alpha_k \mathbf{x}_{k-1}$ ;
4    $\text{agdBrk} \leftarrow \text{AccBreak}(\{\mathbf{x}_k, \mathbf{x}_k^{ag}, \mathbf{x}_k^{md}\}, \Psi, \mathcal{L}_\Psi)$ ;
5   if  $\text{agdBrk}$  or  $k \geq N_{ag}$  or converge to  $\mathcal{F}_{tol}, \theta_{tol}$ 
6     then return  $\mathbf{x}_k^{md}$ .
7   Compute  $\nabla \Psi(\mathbf{x}_k^{md})$  and update  $\{\alpha_k, \beta_k, \lambda_k\}$ ;
8    $\mathbf{x}_k = \mathbf{x}_{k-1} - \lambda_k \nabla \Psi(\mathbf{x}_k^{md})$ ;
9    $\mathbf{x}_k^{ag} = \mathbf{x}_k^{md} - \beta_k \nabla \Psi(\mathbf{x}_k^{md})$ ;

```

---

**Theorem 1.** *Following Lemma 1 and Algorithm 1, we get condition  $\{\alpha_k, \beta_k, \lambda_k\}$  needs to satisfy according to [11]:*

$$C_k = 1 - \mathcal{L}_\Psi \lambda_k - \frac{\mathcal{L}_\Psi (\lambda_k - \beta_k)^2}{2\alpha_k \Gamma_k \lambda_k} \left( \sum_{\tau=k}^N \Gamma_\tau \right) > 0, \quad (4)$$

to approach the convergence of  $\|\nabla \Psi\|$ :

$$\min_{k=1, \dots, N_{ag}} \|\nabla \Psi(\mathbf{x}_k^{md})\|^2 \leq \frac{\Psi(\mathbf{x}_0) - \Psi^*}{\sum_{k=1}^{N_{ag}} \lambda_k C_k}. \quad (5)$$

Unlike Ghadimi's method using a constant  $\mathcal{L}_\Psi$ , our AGD method inserts  $\text{AccBreak}()$  in line 4 of Algorithm 1 to adaptively terminate the AGD process. Moreover, Section VI will detail the technologies of  $\text{AccBreak}()$  to restart AGD with the reestimated  $\mathcal{L}_\Psi$ , while Section VII will reformulate AGD to resample the trajectory adaptively.

#### IV. PROBLEM FORMULATION

As we treat the robotic motion as a GP, we first review the Gauss-Markov process, and the derivation of the GP prior. Then we illustrate the posterior of the GP prior based on the GP theorem in Section IV-B. Finally, Section IV-C reviews how to construct an objective functional informed by the GP and obstacle factors.

##### A. A Gauss-Markov model

Given the initial state, goal state, and environment information, the motion planning problem is a probabilistic inference. Its prior probabilistic model is formed by a linear time-varying stochastic differential equation (LTV-SDE):

$$\dot{\theta}(t) = \mathbf{A}(t)\theta(t) + \mathbf{u}(t) + \mathbf{F}(t)\mathbf{w}(t), \quad (6)$$

where  $\mathbf{A}$  and  $\mathbf{F}$  are the matrices of linear system and stochastic process correspondingly, and  $\mathbf{u}(t)$  is a system input. The white noise process  $\mathbf{w}(t)$  itself is a GP with zero expectation:

$$\mathbf{w}(t) \sim \mathcal{GP}(\mathbf{0}, \mathbf{Q}_c(t)\delta(t-t')), \quad (7)$$

where  $\mathbf{Q}_c(t)$  is an isotropic power-spectral density matrix. Then we could gain the mean  $\tilde{\mu}(t)$  and covariance  $\tilde{\mathcal{K}}(t, t')$ <sup>1,2</sup> of GP generated by LTV-SDE (6) according to [3]:

$$\tilde{\mu}(t) = \Phi(t, t_0)\mu_0 + \int_{t_0}^t \Phi(t, s)\mathbf{u}(s)ds, \quad (8)$$

$$\tilde{\mathcal{K}}(t, t') = \|\Phi(t, t_0)\|_{\mathcal{K}_0^{-1}}^2 + \int_{t_0}^t \|\Phi(t, s)\mathbf{F}(s)\|_{\mathbf{Q}_c^{-1}(s)}^2 ds, \quad (9)$$

where  $\tilde{t} = \min(t, t')$ ,  $\mu_0$  and  $\mathcal{K}_0$  are the mean and covariance of the initial state, and  $\Phi(t, s)$  is the state transition matrix.

##### B. The GP model for motion planning

After gaining a GP prior via (8) and (9), we now construct the observation system of the state

$$\theta' = \mathbf{C}\theta + \varepsilon_{t'}, \quad \varepsilon_{t'} \sim \mathcal{N}(\mathbf{0}, \mathcal{K}'), \quad (10)$$

where the state

$$\theta = [\theta_t^T, \theta_{t+1}^T, \dots, \theta_{t'}^T]^T \sim \mathcal{N}(\tilde{\mu}, \tilde{\mathcal{K}}),$$

$t' \subseteq t = \{t, t+1, \dots, t'\}$ , and  $\mathbf{C}$  denotes the corresponding observation matrix of  $t'$ . Unlike GPMP [3] arbitrarily setting  $\{\theta_t, \theta_{t'}\} = \{\theta_0, \theta_g\}$  and  $\mathbf{C} = [\mathbf{0}_{t_0}, \dots, \mathbf{0}_{t_{N-1}}, \mathbf{I}]$  with  $t' = t_N$ , we alternate the setting of  $\mathbf{C}$  and  $\{t, t'\}$  according to the prerequisites, especially in the BTI case (Section VIII). Based on that, we define the joint distribution as

$$\begin{pmatrix} \theta \\ \theta' \end{pmatrix} \sim \mathcal{N}\left(\begin{bmatrix} \tilde{\mu} \\ \mathbf{C}\tilde{\mu} \end{bmatrix}, \begin{bmatrix} \tilde{\mathcal{K}} & (\mathbf{C}\tilde{\mathcal{K}})^T \\ \mathbf{C}\tilde{\mathcal{K}} & \mathbf{C}\tilde{\mathcal{K}}\mathbf{C}^T + \mathcal{K}' \end{bmatrix}\right).$$

So we formulate the posterior of  $\theta$  given the observation  $\theta'$  and simplify its expression  $\mu_{\theta|\theta'}, \mathcal{K}_{\theta|\theta'}$  by  $\mu, \mathcal{K}$ :

$$\mu = \tilde{\mu} + (\mathbf{C}\tilde{\mathcal{K}})^T(\mathbf{C}\tilde{\mathcal{K}}\mathbf{C}^T + \mathcal{K}')^{-1}(\theta' - \mathbf{C}\tilde{\mu}), \quad (11)$$

$$\mathcal{K} = \tilde{\mathcal{K}} - \tilde{\mathcal{K}}^T \mathbf{C}^T (\mathbf{C}\tilde{\mathcal{K}}\mathbf{C}^T + \mathcal{K}')^{-1} \mathbf{C}\tilde{\mathcal{K}}. \quad (12)$$

<sup>1</sup>This paper uses the bold font, such as  $\theta_{t,t'}, \mu_{t,t'}, \mathcal{K}_{t,t'}$ , for a point in the trajectory space of the time interval  $(t, t')$ , while uses the normal font, such as  $\theta_t, \mu_t, \mathcal{K}_t$ , for a point in configuration space at time  $t$ .

<sup>2</sup>This paper uses  $\|\mathbf{p}\|_{\mathbf{S}}$  to measure the Mahalanobis distance of  $\mathbf{p}$  with the covariance  $\mathbf{S}$ :  $\sqrt{\mathbf{p}^T \mathbf{S}^{-1} \mathbf{p}}$ .

##### C. Cost functionals

This paper adopts the objective functional proposed in [1] for generating an optimal trajectory with low energy cost without collision. In this way, the problem for collision-free optimal motion planning can be formularized as

$$\begin{aligned} & \text{minimize} && \mathcal{F}_{gp}(\theta) \\ & \text{subject to} && \mathcal{G}_i(\theta) \leq 0, \quad i = 1, \dots, m_{ieq} \\ & && \mathcal{H}_i(\theta) = 0, \quad i = 1, \dots, m_{eq}, \end{aligned} \quad (13)$$

where  $\mathcal{F}_{gp}$  is an objective functional for trajectory smoothing,  $\mathcal{G}_i$  is an inequality constraint for collision avoidance,  $\mathcal{H}_i$  is an equality constraints for task requirements.

Since AGP-STO mainly focuses on trajectory optimization whose initial value always dissatisfies  $\mathcal{G}$ , we design the objective functional as

$$\mathcal{F}(\theta) = \mathcal{F}_{obs}(\theta) + \mathcal{F}_{gp}(\theta), \quad (14)$$

where the GP prior  $\mathcal{GP}(\mu, \mathcal{K})$  forms the smooth part

$$\mathcal{F}_{gp}(\theta) = \frac{1}{2} \|\theta - \mu\|_{\mathcal{K}}^2, \quad (15)$$

and the obstacle part  $\mathcal{F}_{obs}$  [1], [3] computes the integration of the body-point kinetic costs in W-space:

$$\mathcal{F}_{obs}(\theta) = \int_{t_0}^{t_N} \varrho(t) \int_{\mathcal{B}} c[\mathbf{x}(u, t)] \|\dot{\mathbf{x}}(u, t)\| du dt, \quad (16)$$

where factor  $\varrho(t)$  penalizes the collision-free constraints  $\mathcal{G}_i$ ,  $c(\cdot) : \mathbb{R}^3 \rightarrow \mathbb{R}$  gathers the obstacle information of the set of points  $\mathcal{B} \subset \mathbb{R}^3$  on the robot body in W-space, and  $x$  maps from C-space to W-space via the forward kinematics.

Now some readers might query about the relation between the functional  $\mathcal{F}(\theta)$  and the probabilistic inference of  $\theta$ . Here we define a posterior  $p(\theta|\theta', \mathcal{G})$  informed by the obstacle  $\mathcal{G}$  and the GP prior formulated in Section IV-B:

$$p(\theta|\theta', \mathcal{G}) = \frac{1}{\mathcal{P}} \exp \left\{ -\frac{1}{2} \|\theta - \mu\|_{\mathcal{K}}^2 - \mathcal{F}_{obs}(\theta) \right\},$$

where  $\mathcal{P} = \int_{\theta \in \Theta} e^{-\mathcal{F}(\theta)} d\theta$ <sup>3</sup>, and  $\varrho(t)$  adjusted by the penalty method (Section V) gathers the GP prior and obstacle information. Then we could gain an optimum

$$\theta^* = \operatorname{argmax}_{\theta \in \Theta} p(\theta|\theta', \mathcal{G}) \quad (17)$$

via MAP and obtain  $\mathcal{F}(\theta)$  via  $-\log p(\theta|\theta', \mathcal{G})$ .

#### V. ADAPTIVE GAUSSIAN PROCESS BASED STOCHASTIC TRAJECTORY OPTIMIZATION

Trajectory optimization primarily finds an optimal solution via finding a Hamiltonian minimum. This paper utilizes the time discretization method [3] to represent the time-continuous trajectory  $\theta$  by  $[\theta_0^T, \dots, \theta_N^T]^T$ . In this way, our method, AGP-STO, in Figure 2, maximizes the posterior  $p(\theta|\theta', \mathcal{G})$  (17) for optimization. To solve the above MAP problem, this section first presents the intuition of our methodology, then illustrates the scheme of AGP-STO integrating the numerical and sampling method.

<sup>3</sup> $\Theta$  denotes a feasible set of  $\theta$  under the motion constraint (47).

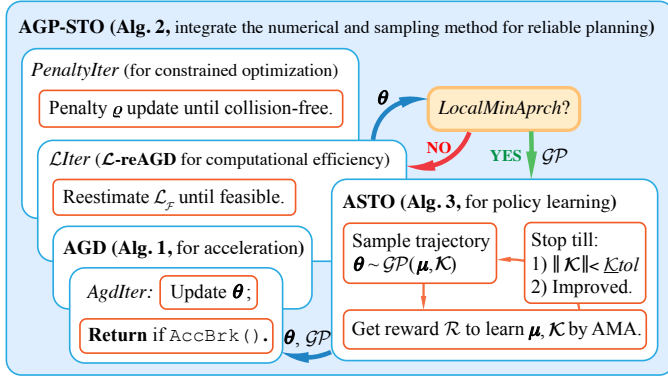


Fig. 2: A block diagram illustrates how AGP-STO (Algorithm 2) plans an optimal motion in a cluttered W-space and how the numerical ( $\mathcal{L}$ -reAGD, Section VI) and sampling (ASTO, Algorithm 3) methods are integrated to solve the nonconvex optimization problem.

### A. Intuition

CHOMP [1] gives an example of a super-ball rolling on a landscape until exhausting the kinetic energy to illustrate how CHOMP utilizes the HMC method to approach the optimum. This section adopts the example and provides the intuition behind AGP-STO in Figure 2 & 3. In our mind, two main concerns exist in CHOMP: (i) how to resample a stochastic momentum to drive a super-ball towards the optimum with high probability in a trajectory space; (ii) how to define an energy field whose total value contains the potential and kinetic energy to roll the ball towards the minima efficiently.

GPMP2 [3] sends the blue ball (Figure 3) off a hill downwards the nearest valley (Local Minima-1) with a few steps, calculated via the LM method utilizing the Gauss kernel to transform the gradient. In comparison, CHOMP accumulates the kinetic via the rejection sampling and moves following the differential equation derived from a Hamiltonian

$$\mathfrak{H}(\theta) = \mathfrak{K}(\theta) + \mathcal{F}(\theta). \quad (18)$$

It contains a kinetic part  $\mathfrak{K} = \frac{\mathcal{L}_{\mathcal{F}} \|\dot{\theta}\|^2}{2}$ <sup>4,5</sup> and a potential part  $\mathcal{F}$  to overcome a wavy terrain nearby the Local Minima-1 in Figure 3. However, CHOMP still easily rolls the red ball downwards the Local Minima-2.

So why cannot we learn the momenta associated with its kinetic energy  $\mathfrak{K}$  directly from its potential energy  $\mathcal{F}$  when facing the nonconvex cases? ASTO (Algorithm 3) actuates the green ball of Figure 3 by the expected value of the sampled momenta obeying the Gauss distribution in proportion to  $\exp(-\zeta \mathfrak{K})$  with a flatten factor  $\zeta$ . Moreover, it renews the Gauss model associated with  $\mathfrak{K}$  to resample the momenta performing better in ball motivation and then actuates the green ball repeatedly until the expected momentum becomes zero or the ball rolls into the convex subspace. After that,  $\mathcal{L}$ -reAGD which generalizes the leapfrog method stimulates the ball motion until  $\{\mathfrak{K}, \|\nabla \mathcal{F}\|\} \rightarrow 0$ . Unlike CHOMP reserving  $\mathfrak{K}$  from a constant prior distribution, our method adaptively restarts the AGD with zero  $\mathfrak{K}$  and a reestimated inertia  $\mathcal{L}_{\mathcal{F}}$  to

<sup>4</sup> $\mathcal{L}_{\mathcal{F}}$  is the Lipschitz constant of the objective functional  $\mathcal{F}$ .

<sup>5</sup> $\dot{\theta}$  denotes the trajectory variation rate during the optimization rather than its higher derivation with respect to time  $t$  of trajectory.

improve the movement efficiency. Considering  $\mathcal{G}$  (17), AGP-STO adopts the penalty method when the robot confronts the collision risk to adjust the potential field  $\mathcal{F}$  with  $\rho$  (16).

In conclusion, AGP-STO (i) utilizes the stochastic momenta, reserving the kinetic energy, by ASTO (Section VII) to overcome the highly wavy landscape (i.e., the high non-convexity) around the global optimum; (ii) restarts the AGD movement (Section VI) driven by  $\mathcal{L}_{\mathcal{F}}$  to improve the descent rate; (iii) integrates the penalty and Lagrangian augmentation method (Section V-B), adjusting the potential field determined by  $\mathcal{F}$ , to meet the inequality constraints.

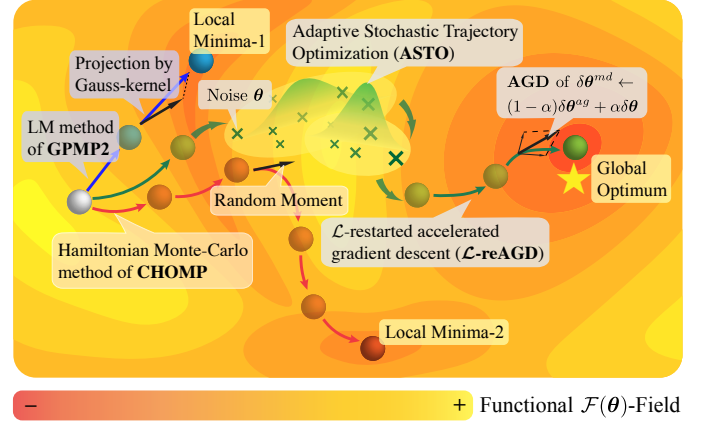


Fig. 3: An example of a super-ball, rolling in a trajectory-space, illustrates how AGP-STO (Algorithm 2), CHOMP [1], and GPMP2 [3] search for an optimal solution via momentum descent. The green trace shows how AGP-STO rolls a green ball into the global optimum by the mixed momentum from  $\mathcal{L}$ -reAGD (Section VI) and ASTO (Algorithm 3). The blue trace shows how GPMP2 rolls a blue ball into a local minimum by a determinant speed with an acceleration (Gauss-kernel). The red trace shows the resampled speed of CHOMP rolling a red ball into a local minimum.

### B. AGP-STO for Maximum A Posterior

The above demonstrates an example of how a super-ball, rolls towards the lowest valley of the potential field determined by  $\mathcal{F}$  to give an interpretation of how AGP-STO plans an optimal motion. Someone may ask about the alternative perspective of the MAP of  $p(\theta|\theta', \mathcal{G})$ . Section IV-C gives the relation between the objective functional  $\mathcal{F}$  and  $\theta$ 's posterior informed by the GP prior and other constraints  $\mathcal{G}$ . It indicates  $p(\theta|\theta', \mathcal{G})$  attaches the maximum when the super ball is trapped in a local minimum. Besides, the kinetic energy  $\mathfrak{K}$  denotes a prior probability distribution of the optimization step. So that ASTO and  $\mathcal{L}$ -reAGD can infer the posterior via adaptive resampling and the restarted AGD.

AGP-STO (Algorithm 2) adopts a frame with the nested loops for the MAP of  $p(\theta|\theta', \mathcal{G})$ . The outer loop (*Penlter*) adjusts the penalty factor  $\rho$  for the collision-free trajectory inference. Since we use the discretization form of (14):

$$\mathcal{F}(\theta) = \frac{1}{2} \|\theta - \mu\|_{\mathcal{K}} + \sum_{t=t_0}^{t_g} \sum_{B_i \in \mathcal{B}} \rho(t) c[\mathbf{x}_i(t)] \|\dot{\mathbf{x}}_i(t)\| \quad (19)$$

for the constrained optimization of discretized trajectory  $\theta = [\theta_0^T, \dots, \theta_N^T]^T$ , we increase  $\rho = [\rho_0, \dots, \rho_N]^T$  corresponding to  $\theta$  until the trajectory satisfies the constraints  $\mathcal{G}_{\text{tol}}$ . In the

second loop ( $\mathcal{L}Iter$ , Section VI-B), we restart the AGD process with the reestimated  $\mathcal{L}_{\mathcal{F}}$  ( $\mathcal{L}$ -reAGD) rather than the size adjustment of the trust region to solve the semi-convex problem when the improvement exceeds the threshold. Furthermore, AGP-STO employs ASTO (Section VII, Figure 6) in  $\mathcal{L}Iter$  when the MAP approaches a local minimum.

---

**Algorithm 2: AGP-STO**


---

**Input:** initial trajectory  $\theta_0$ , prior  $\mathcal{GP}(\mu_0, \mathcal{K}_0)$ , factor  $\varrho$ , and objective functional  $\mathcal{F}[\theta(t)]$ .

1 **Initialize:**  $\theta \leftarrow \theta_0$ , initial Lipschitz constant  $\mathcal{L}_{\mathcal{F}}$ , update rules  $\{\alpha, \beta, \gamma\}$  of AGD, penalty scaling factor  $\kappa$ , convergence thresholds  $\mathcal{F}tol, \theta tol$ ;

2 **for**  $PenIter : i = 1 \dots N_{\varrho}$  **do**

3     **for**  $\mathcal{L}Iter : j = 1 \dots N_{\mathcal{L}}$  **do**

4         Reestimate  $\mathcal{L}_{\mathcal{F}}$  according to Section VI-B;

5         **if**  $MinAprch()$  **then**

6              $\{\theta, \mathcal{GP}(\mu, \mathcal{K})\} \leftarrow \text{ASTO}(\mathcal{F}, \mathcal{GP}(\theta, \mathcal{K}))$   
            via **Algorithm 3**;

7             Update  $\mathcal{F}$  by (19) and reinitialize  $\mathcal{L}_{\mathcal{F}}$ ;

8          $\theta \leftarrow \text{AGD}(\theta, \mathcal{F}, \mathcal{L}_{\mathcal{F}}, \{\alpha, \beta, \gamma\}, \text{AccBreak}())$   
            via **Algorithm 1**;

9         **if** converge to  $\mathcal{F}tol$  or  $\theta tol$  **then goto** 10;

10     **if**  $\mathcal{F}_{obs}(\theta) < \mathcal{G}tol$  **then return**  $\{\theta, \mathcal{GP}(\mu, \mathcal{K}), \varrho\}$ .

11     **else**  $\varrho \leftarrow \kappa \cdot \varrho$ ;

12 **return**  $\{\theta, \mathcal{GP}(\mu, \mathcal{K}), \varrho\}$ .

---

## VI. $\mathcal{L}$ -REAGD FOR TRAJECTORY OPTIMIZATION

This Section utilizes AGD (Section III-A) for MAP. It generalizes and upgrades HMC adopted by CHOMP to achieve high efficiency and robustness compared to GPMP2. Section VI-A details how to implement AGD and gives Corollary 1 about AGD-step estimation. Considering the variation of the planning scenery during the collision avoidance, Section VI-B proposes an  $\mathcal{L}$ -restart method for AGD-based OMP and provides its physical interpretation. Finally, we propose a method to determine whether the local minimum approaches, combining the collision avoidance progress.

### A. Accelerated Gradient Descent for Trajectory Optimization

The OMP problem (13) contains a class of composite problems (14), where the  $\mathcal{GP}$  functional  $\mathcal{F}_{gp}$  is strongly convex while the obstacle functional  $\mathcal{F}_{obs}$  is always nonconvex (Figure 5). So we implement Algorithm 1 by  $\mathcal{F} \rightarrow \Psi$  for MAP and assume that  $\mathcal{F}$  is semi-convex and continuously differentiable in a subspace

$$\mathcal{C} = \left\{ \theta, \theta' \mid |\mathcal{F} + \langle \bar{\nabla} \mathcal{F}, \theta' - \theta \rangle - \mathcal{F}'| \leq \frac{\mathcal{L}_{\mathcal{F}}}{2} \|\theta' - \theta\|^2 \right\} \quad (20)$$

where  $\mathcal{F}$ ,  $\mathcal{F}'$  and  $\bar{\nabla} \mathcal{F}$  simplify  $\mathcal{F}(\theta)$ ,  $\mathcal{F}(\theta')$  and  $\bar{\nabla} \mathcal{F}(\theta)$  respectively, and  $\langle \cdot, \cdot \rangle$  denotes the inner production. The reason we call it semi-convex is that it does not have to meet the strongly convex condition:

$$\mathcal{F}(\alpha\theta + (1-\alpha)\theta') \leq \alpha\mathcal{F} + (1-\alpha)\mathcal{F}', \alpha \in [0, 1]. \quad (21)$$

The AGD-based MAP utilizes the historical momenta and releases the strict descent of the steepest descent to avoid some infeasible solutions [11] in some nonconvex cases. The benchmark results of Table VI.A shows the solvability and efficiency of  $\mathcal{L}$ -reAGD in some nonconvex cases, comparing to CHOMP and GPMP. Right now, we detail how AGD ( $\theta, \mathcal{F}$ ) makes a trajectory MAP.

**Corollary 1.** *According to Theorem 1 and the definition of  $\mathcal{L}_{\mathcal{F}}$ -convex hull (20), we design  $\alpha_k$  and  $\beta_k$  as*

$$\alpha_k = \frac{2}{k+1}, \quad \beta_k = \frac{1}{\vartheta_1 \mathcal{L}_{\mathcal{F}}}.$$

*Following the constraint of inequality  $C_k > 0$  (4) and the definition of*

$$\lambda_k \in [\beta_k, (1 + \vartheta_2 \alpha_k) \beta_k], \forall k \geq 1,$$

*we can get*

$$\left( \vartheta_2 + \frac{\alpha_k}{2} \right)^2 \leq \vartheta_1 - 1 + \frac{\alpha_k^2}{4}, \quad \vartheta_2 \geq 0$$

*by the substitution of  $\lambda_k$  under the inequality reduction<sup>6</sup>. Then due to (5), we can get the convergence of*

$$\min_{k=1 \dots N_{ag}} \|\bar{\nabla} \mathcal{F}_k^{md}\|^2 \leq \frac{\vartheta_1^2 \mathcal{L}_{\mathcal{F}} (\mathcal{F}_0 - \mathcal{F}_*)}{N_{ag}(-\vartheta_2^2 - \vartheta_2 + \vartheta_1 - 1)}. \quad (22)$$

Now, let us see how the super ball in Figure 3, representing a trajectory, performs an accelerated descent stimulated by Algorithm 1 and analytically compares its performance with CHOMP. According to Algorithm 1, we can get

$$\begin{aligned} & \frac{k}{2} (\theta_{k+1}^{md} - 2\theta_k^{md} + \theta_{k-1}^{md}) + \left( \theta_{k+1}^{md} - \frac{\theta_k^{md} + \theta_{k-1}^{md}}{2} \right) \\ &= -\frac{k}{2} (\beta_k \bar{\nabla} \mathcal{F}_k^{md} - \beta_{k-1} \bar{\nabla} \mathcal{F}_{k-1}^{md}) - \lambda_k \bar{\nabla} \mathcal{F}_k^{md} - \frac{\beta_{k-1}}{2} \bar{\nabla} \mathcal{F}_{k-1}^{md}. \end{aligned}$$

It can be transformed to an ordinary differential equation (ODE) due to Corollary 1 when  $\vartheta_1 = \delta_{\tau}^{-1}$  and  $\delta_{\tau} \rightarrow 0$ :

$$\frac{d^2 \theta}{d\tau^2} + \frac{3 d\theta}{\tau d\tau} = -\frac{1}{\mathcal{L}_{\mathcal{F}}} \left( 1 - \frac{1}{\tau} \right) \frac{d\bar{\nabla} \mathcal{F}}{d\tau} - \frac{1}{\mathcal{L}_{\mathcal{F}} \tau} \bar{\nabla} \mathcal{F} \quad (23)$$

where  $\tau = k\delta_{\tau}$  denotes the optimization time of AGD process. The above ODE indicates our method approximately solves the first order system. In comparison, the leapfrog method solves the second order system

$$d^2 \theta / d\tau^2 = -\mathcal{L}_{\mathcal{F}}^{-1} \bar{\nabla} \mathcal{F}, \quad (24)$$

which is attained via setting  $\lambda_k = \alpha_k^{-1} \beta_k$ . However, its update rule results in a series of negative  $\{C_k\}$  of (4) and the corresponding AGD ( $\cdot$ ) converges with the rate

$$\mathcal{F}_N^{ag} - \mathcal{F}^* \leq \frac{2\vartheta_1 \mathcal{L}_{\mathcal{F}} \|\theta_0 - \theta^*\|^2}{N_{ag}(N_{ag} + 1)} \quad (25)$$

rather than (22)'s rate. However, it requires a strong convexity (21) or high inertia (i.e., large  $\mathcal{L}_{\mathcal{F}}$ ) to ensure the system's stability according to [11], [41]. These requirements can resist the capacity of overcoming the potential field's fluctuation and lower the success rate. That is the reason why Corollary 1,

<sup>6</sup>Appendix A elaborates the detailed information

rather than [41]'s method, is utilized in  $\text{AGD}()$ . Section X-B1 compares  $\mathcal{L}$ -reAGD with CHOMP to validate our choice.

Unlike CHOMP which gains an initial momentum by Monte-Carlo sampling, the AGD method rolls the ball with constant inertia  $\mathcal{L}_{\mathcal{F}}$  obeying (20) from the zero initial in a smooth landscape. For both of them, the constant inertia determines the ball's resistance to the velocity change by force from the potential field. It means the external force  $\bar{\nabla}\mathcal{F}$  could affect the trace of the light ball more quickly than the heavy one. So a proper selection of  $\mathcal{L}_{\mathcal{F}}$  highly determines an effective descent towards a minimum. The following subsection will detail how to estimate  $\mathcal{L}_{\mathcal{F}}$  precisely and how the  $\mathcal{L}$ -restart method adaptively restarts the AGD-process.

### B. $\mathcal{L}$ -Restart of Accelerated Gradient Descent

When the robot of Figure 4 avoids an obstacle in W-space, the designed collision field  $c(\mathbf{x})$  of (16) will provide a repulsive force to push  $\mathcal{B}_i$ 's body, denoted by the red ball, away from the unsafe area. Since (19) treats the body avoidance process as the movement of a series of geometrically connected collision-check balls (CCBs) repelled by force. So how the force affects these CCBs determines how effective the collision avoidance is. Figure 4 demonstrates how the AGD-restart happens when the repelled part varies from  $\{\mathcal{B}_1, \mathcal{B}_2\}$  to  $\{\mathcal{B}_1\}$ . When the joint force pushes  $\mathcal{B}_1$  and  $\mathcal{B}_2$ , larger inertia ensures the super ball rolling stably. After  $\mathcal{B}_2$  avoids the collision, the large inertia will dampen  $\mathcal{B}_1$ 's movement. In conclusion, the various combinations of the activated CCBs could lead to various  $\mathcal{L}_{\mathcal{F}}$  affecting the descent efficiency. So this section will first propose the methodology of  $\mathcal{L}_{\mathcal{F}}$ -estimation and AGD-restart, then introduce how to decide the local minimum approaches.

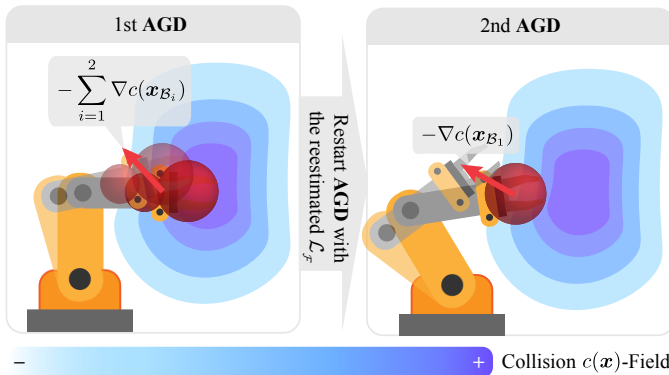


Fig. 4: An example demonstrates how the repulsive force (red arrow) from the collision field  $c(\mathbf{x})$  (blue contour map) effects the robot arm by repelling the collision check ball (CCB, red sphere) and how  $\mathcal{L}$ -reAGD restarts AGD with the reestimated  $\mathcal{L}_{\mathcal{F}}$ .

CHOMP [1] and iSAGO [41] set initial inertia arbitrarily and expand it exponentially to progressively weaken the ball's response to the potential field during movements. While GPMP [3] estimates the inertia matrix consisted of mass and rotational inertia based on the LM method to move the ball efficiently. Unlike the above methods,  $\mathcal{L}$ -reAGD restarts the AGD process with the reestimated mass, when the descent performance exceeds expectations. Though some recent studies [11], [41], [57]–[59] focus on AGD-restart to promote the

descent rate, most of them design a warm restart scheme and estimate  $\mathcal{L}_{\mathcal{F}}$  with arbitrary expanding or shrink. Our method constructs  $\mathcal{C} = \bigcup_{j=1}^{N_c} \mathcal{C}_j$  with the reestimated  $\mathcal{L}_{\mathcal{F}}^{(j)}$  based on (20). Since a hull  $\mathcal{C}$  with a larger  $\mathcal{L}_{\mathcal{F}}$  contains a hull with a smaller  $\mathcal{L}_{\mathcal{F}}$ , some AGD methods proven optimal for 1st-order descent in some convex cases still perform poorly with an improper  $\mathcal{L}_{\mathcal{F}}$ . Section X-B1 validates that  $\mathcal{L}$ -reAGD performs more efficiently than AGD with a constant  $\mathcal{L}_{\mathcal{F}}$ .

To improve AGD, we insert  $\text{AccBreak}(\theta_k^{md}, \mathcal{F}, \mathcal{L}_{\mathcal{F}})$  at Line 5 of Algorithm 1 to evaluate the step performance and adaptively restart AGD. According to (20) and Section III-A, our method first defines the predicted reduction

$$\begin{aligned} \text{pred}_{\text{low}} &= \langle \bar{\nabla}\mathcal{F}_{k-1}, \theta_k - \theta_{k-1} \rangle + \frac{c_{\text{low}}\mathcal{L}_{\mathcal{F}}}{2} \|\theta_k - \theta_{k-1}\|^2 \\ \text{pred}_{\text{up}} &= \langle \bar{\nabla}\mathcal{F}_{k-1}, \theta_k - \theta_{k-1} \rangle - \frac{c_{\text{up}}\mathcal{L}_{\mathcal{F}}}{2} \|\theta_k - \theta_{k-1}\|^2 \end{aligned} \quad (26)$$

and then designs

$$\text{AccBreak}(\theta_k^{md}, \mathcal{F}, \mathcal{L}_{\mathcal{F}}) = \begin{cases} \text{True} & \text{if } \text{ared} > \text{pred}_{\text{low}} \\ \text{True} & \text{if } \text{ared} < \text{pred}_{\text{up}} \\ \text{False} & \text{Otherwise,} \end{cases} \quad (27)$$

where  $\text{ared} = \mathcal{F}_{k-1} - \mathcal{F}_k$  denotes the actual reduction. Besides,  $\text{ared} > \text{pred}_{\text{low}}$  means AGD performs with insufficient reduction, while  $\text{ared} < \text{pred}_{\text{up}}$  means  $\mathcal{L}_{\mathcal{F}}$  resists the AGD-step. So the both conditions can activate the restart process with the reestimated  $\mathcal{L}_{\mathcal{F}}$ . Next, we will introduce how to reestimate  $\mathcal{L}_{\mathcal{F}}$  facing these two conditions.

1)  $\text{ared} > \text{pred}_{\text{low}}$ : Based on Corollary 1 and (20), we could gain a prerequisite an AGD-step needs to satisfy within a proper hull  $\mathcal{C}(\mathcal{L}_{\mathcal{F}})$ :

$$\begin{aligned} \mathcal{F}_{k-1} - \mathcal{F}(\theta_{k-1} - \frac{1+\vartheta_2}{\vartheta_1\mathcal{L}_{\mathcal{F}}} \bar{\nabla}\mathcal{F}_k) &\geq \frac{\varpi_k}{\mathcal{L}_{\mathcal{F}}}, \\ \varpi_k &= \frac{2\vartheta_2+k+1}{\vartheta_1(k+1)} \left( 1 - \frac{2\vartheta_2+k+1}{\vartheta_1(k+1)} - \frac{\vartheta_2^2}{\vartheta_1} \right) \|\bar{\nabla}\mathcal{F}_k\|^2. \end{aligned}$$

When the above relationship does not hold, a renewed  $\mathcal{L}_{\mathcal{F}}$  will reconstruct another hull  $\mathcal{C}$ . To renew  $\mathcal{L}_{\mathcal{F}}$ , we first define

$$\phi(\mathcal{L}_{\mathcal{F}}) = \mathcal{F}(\theta_{k-1} - \frac{1+\vartheta_2}{\vartheta_1\mathcal{L}_{\mathcal{F}}} \bar{\nabla}\mathcal{F}_k) - \mathcal{F}(\theta_{k-1}).$$

Since a low resistant (i.e. a small  $\mathcal{L}_{\mathcal{F}}^{(j)}$ ) to exterior force leads to the unacceptable movement of the super-ball. It is reasonable to say the renewed semi-convex hull  $\mathcal{C}_{j+1}$  contains the former hull  $\mathcal{C}_j$ , meaning that  $\mathcal{L}_{\mathcal{F}}^{(j+1)} \in (\mathcal{L}_{\mathcal{F}}^{(j)}, \infty)$ . So we formulate a quadratic approximation function

$$\phi_q(\mathcal{L}_{\mathcal{F}}) = \frac{\mathcal{L}_{\mathcal{F}}^{(j)} \phi(\mathcal{L}_{\mathcal{F}}^{(j)}) - \frac{1+\vartheta_2}{\vartheta_1} \dot{\phi}(\infty)}{\mathcal{L}_{\mathcal{F}}^2 / \mathcal{L}_{\mathcal{F}}^{(j)}} + \frac{1+\vartheta_2}{\vartheta_1\mathcal{L}_{\mathcal{F}}} \dot{\phi}(\infty)$$

like the line search methods [12], [34]. Unlike these methods, however, our algorithm only approximates  $\phi(\mathcal{L}_{\mathcal{F}})$  in the quadratic (i.e., second-order) form and abandons their higher-order form, considering the computational cost. Then we can update  $\mathcal{L}_{\mathcal{F}}$  via solving

$$\arg\min_{\mathcal{L}_{\mathcal{F}}} \phi_q(\mathcal{L}_{\mathcal{F}}) + \frac{\varpi_k}{\mathcal{L}_{\mathcal{F}}}$$

and obtain

$$\frac{\mathcal{L}_{\mathcal{F}}^{(j+1)}}{\mathcal{L}_{\mathcal{F}}^{(j)}} = \frac{\mathcal{L}_{\mathcal{F}}^{(j)} \phi(\mathcal{L}_{\mathcal{F}}^{(j)}) - \frac{1+\vartheta_2}{\vartheta_1} \dot{\phi}(\infty)}{-\frac{1}{2} \left( \frac{1+\vartheta_2}{\vartheta_1} \dot{\phi}(\infty) + \varpi_k \right)}. \quad (28)$$

The above  $\mathcal{L}_{\mathcal{F}}$ -reestimation will perform sequentially till the condition  $ared \leq pred_{low}$  is satisfied.

The above method adjusts  $\mathcal{L}_{\mathcal{F}}$  iteratively, only calculating  $\dot{\phi}(\infty)$  for once. Its utilization occurs when the AGD-step is rejected initially within  $\mathcal{C}_j$ . However, it requires the negative-definite of  $\dot{\phi}(\infty)$  to ensure the positive definite of the renewed  $\mathcal{L}_{\mathcal{F}}$ . So how to deal with the semi-negative definition situation? An intuition that directly finds the constraint's boundary could satisfy the condition. In this way, we gain

$$\mathcal{L}_{\mathcal{F}}^{(j+1)} = \frac{ared + \langle \bar{\nabla} \mathcal{F}_{k-1}^{md}, \theta_{k-1}^{md} - \theta_k^{md} \rangle}{\frac{1}{2} c_{low} \|\theta_k^{md} - \theta_{k-1}^{md}\|^2}. \quad (29)$$

2)  $ared < pred_{up}$ : Unlike the above condition, urging for a sufficient reduction, this condition indicates the inertia (i.e.,  $\mathcal{L}_{\mathcal{F}}$ ) resists the AGD process. To modify this poor condition, we first observe how the force  $\|\bar{\nabla} \mathcal{F}\|$  variants with respect to the change of position  $\|\theta\|$  and then modify  $\mathcal{L}_{\mathcal{F}}$  to meet the  $\mathcal{L}_{\mathcal{F}}$ -continuous requirement (20) of  $\bar{\nabla} \mathcal{F}$ . Based on that, we could get the upper bound:

$$\mathcal{L}_{\mathcal{F}}^{(j+1)} \leq \frac{\|\bar{\nabla} \mathcal{F}_k^{md} - \bar{\nabla} \mathcal{F}_{k-1}^{md}\|}{c_{up} \|\theta_k^{md} - \theta_{k-1}^{md}\|}. \quad (30)$$

Similar to (29), we could get the lower bound:

$$\mathcal{L}_{\mathcal{F}}^{(j+1)} \geq \frac{\langle \bar{\nabla} \mathcal{F}_{k-1}^{md}, \theta_k^{md} - \theta_{k-1}^{md} \rangle - ared}{\frac{1}{2} c_{up} \|\theta_k^{md} - \theta_{k-1}^{md}\|^2}, \quad (31)$$

according to (20) and (26). In this way, our method iteratively resamples the  $\mathcal{L}_{\mathcal{F}}$  between the lower (31) and upper (30) bound until  $ared \geq pred_{up}$ .

3) *Local minimum approach*: Though the obstacle cost function  $c(\mathcal{D})$  designed in Section IX-B is twice-differential continuity, the overall cost function (Figure 5) is usually first-order differential discontinuity when the obstacle is relatively narrow compared to the robot itself. It means that the objective functional  $\mathcal{F}$  is strongly nonconvex. We call it strong because it is formed by the steep valley of  $\mathcal{F}$  rather than the low fluctuation that satisfies (20) and can be overcome by Corollary 1.  $\mathcal{L}$ -reAGD will adaptively expand  $\mathcal{L}_{\mathcal{F}}$  large enough to descend robustly by confronting the steep valley leading to a local minimum. However robustly the steps perform, they could not change the fact that the process finally approaches the local minimum. So it is meaningful to detect the local minimum approach (MinAprch) and find a way to avoid it.

Our former study [41] measures the included angle between the activated CCBs and assumes MinAprch when the angle is out of acceptance. It is useful, especially when implementing the robot with the serially connected CCBs. However, it highly depends on how the CCBs are connected, and it is sometimes incompatible with the parallel connection case, such as the multi-vehicle allocation in Section X-E.

This paper studies the body-obstacle stuck case shown in Figure 5 and proposes MinAprch() to determine the local

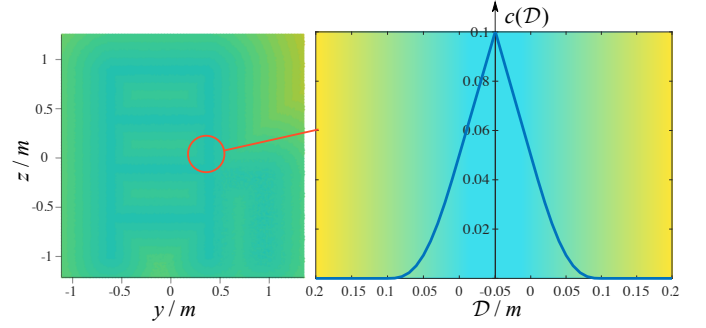


Fig. 5: An example shows the signed distance (the color lightens from blue to yellow with the signed value increasing) and the curve of collision cost generated via (46). The triangular-shaped part illustrates the differential discontinuity of the collision cost field in the corridor case.

minimum approaches. When the robot is stuck in an obstacle, we will see whichever direction the robot moves in within hull  $\mathcal{C}$ , and the functional cost  $\mathcal{F}$  will stay invariant or even grows. In such a case, the curvature of the descent step will become negative, meaning there both exists hill and valley within hull  $\mathcal{C}$  shown in Figure 5. Another phenomenon that the over-expanded  $\mathcal{L}_{\mathcal{F}}$  could not perform an acceptable descent also indicates MinAprch. In this way, we design

$$\text{MinAprch}() = \begin{cases} \text{True} & \text{if } \dot{\phi} \geq |ared| \cdot \phi_{tol} \\ \text{True} & \text{if } \mathcal{L}_{\mathcal{F}}^{(j+j)} \geq \mathcal{L}_{\mathcal{F}}^{(j+1)} \mathcal{L}_{tol} \\ \text{False} & \text{Otherwise,} \end{cases} \quad (32)$$

where  $\phi_{tol}$  prevents the AGD-step from the negative curvature,  $\mathcal{L}_{tol}$  avoids the over-expanded  $\mathcal{L}_{\mathcal{F}}$ , and  $j > 1 \in \mathbb{N}$  is the loop-index for the sequential estimation from  $\mathcal{L}_{\mathcal{F}}^{(j)}$ . Someone may ask why we choose  $j > 1$  than  $j \geq 1$ ? Because  $\mathcal{L}$ -reAGD arbitrarily initializes  $\mathcal{L}_{\mathcal{F}} = \|\bar{\nabla} \mathcal{F}\|$  after ASTO or AGD-restart. So it is rational to take  $\mathcal{L}_{\mathcal{F}}^{j+1}$  as the reference value and choose  $j > 1$  to judge whether  $\mathcal{L}_{\mathcal{F}}$  is over-expanded.

When MinAprch() returns **True** in Line 5 of Algorithm 2, AGP-STO will stimulate ASTO (Section VII, Algorithm 3) to find a semi-convex subspace nearby the optimum. Section X-D validates that it saves the computational resource consumed for the extra iterations for an acceptable  $\mathcal{C}$  and elevates the success rate via sampling-based motion planning.

## VII. ADAPTIVE STOCHASTIC TRAJECTORY OPTIMIZATION

This section proposes an adaptive stochastic trajectory optimization (ASTO) algorithm inspired by STOMP [7]. ASTO involves stochastic trajectory optimization using the noisy trajectories sampled from the adaptive Gaussian distribution. Unlike STOMP whose Gaussian covariance represents the sum of squared acceleration, we utilize the GP model

$$\begin{aligned} & \underset{\theta(t,t')}{\text{minimize}} && \mathcal{F}[\theta(t,t')] \\ & \text{subject to} && \theta(t,t') \sim \mathcal{GP}(\mu(t,t'), \mathcal{K}(t,t')). \end{aligned}$$

to gain the prior knowledge of the trajectory distribution like [52] and interact with the potential field  $\mathcal{F}(\theta)$  to learn the optimal policy adaptively via trajectory sampling.

Continuing the interpretation of AGP-STO in Section V-A, we treat ASTO (Figure 6) as reinforcement learning (RL).

The RL-based process activates the super-ball, representing the trajectory, to learn the  $\mathcal{F}$ -field policy (i.e., GP model). During the interaction, ASTO resamples the trajectories sequentially and evaluates their potential energy to reward. During the RL rewarding, we first adopt the arithmetic operator in [7] and conduct an exponential measurement of the sampled trajectories. Then we utilize the expectation-maximization (EM) method in Section VII-A to gain a reward. To improve the learning progress, we propose an accelerated moving averaging (AMA, Section VII-B) method based on AGD (Section III-A), which generalizes and reformulates the exponential moving averaging (EMA) method.

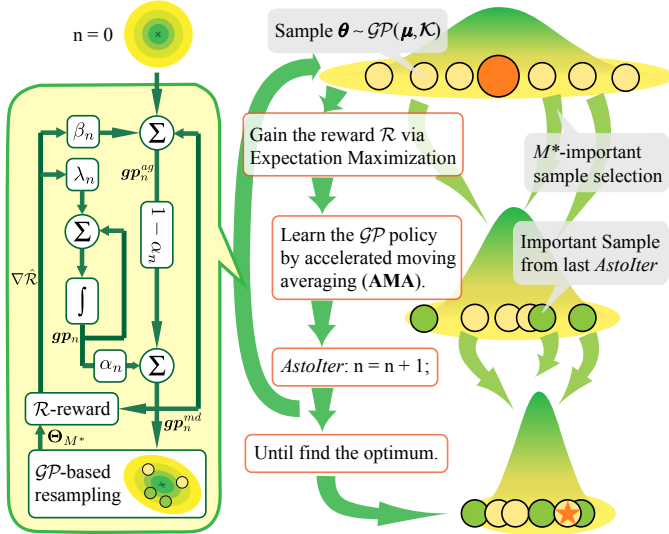


Fig. 6: A system diagram on the left side shows how ASTO applies AGD to perform an AMA process during resampling and adaptively learns a GP policy. The right side demonstrates how to select  $M^*$  important samples with low  $\mathcal{F}$ -cost and utilize them to renew the GP model via AMA.

#### A. Expectation-Maximization for GP-learning

This Section utilizes the adaptive GP and EM [60] method to construct RL's reward and learning strategy. AGPR [61] constructs sliding windows to make a model-free prediction. Unlike AGPR learning from the priorly collected and labeled dataset, ASTO gains the dataset  $\Theta_K$  labeled by  $\mathfrak{F}_K$  via interacting with the field  $\mathcal{F}$  (i.e., online sampling and evaluation). Moreover, the  $\mathcal{R}$ -rewarding proceeds by the EM method.

During the interaction, ASTO (Algorithm 3) first samples a set  $\Theta_K$  consisting of  $K$  sampled trajectories  $\theta_k$  obeying  $\mathcal{GP}(\mu, \mathcal{K})$ . Then it confines each sample in the motion constraints (Section IX-C). Since a large  $\mathcal{K}$ -norm can invoke the sample aggregation nearby the motion constraints, we sample the trajectories obeying the uniform distribution  $\mathcal{U}(\theta_{\min}, \theta_{\max})$  when the covariant norm is beyond the upper threshold  $\bar{\mathcal{K}}tol$  for a more comprehensive gathering of environmental information. After that, it evaluates each sample's potential energy  $\mathcal{F}(\theta_k)$  and gathers them in the set  $\mathfrak{F}_K$ .

So far, ASTO has performed the action based on the policy  $\mathcal{GP}(\mu, \mathcal{K})$  and gathered environment information  $\mathfrak{F}_K$ . Now it is time to gain the reward from the interaction. ASTO adopts the EM method to gain the rewards for policy learning

#### Algorithm 3: ASTO

---

**Input:** functional  $\mathcal{F}$  and prior  $\mathcal{GP}(\mu_0, \mathcal{K}_0)$ ;  
**Initialize:**  $\{\mu_1^{md}, \mathcal{K}_1^{md}\} = \{\mu_0, \mathcal{K}_0\}$ ,  $K = K_0$ ,  
 $\mathfrak{F}_K = \emptyset$ ,  $\Theta_K = \emptyset$ ;  
**for** *Astolter*:  $n = 1 \dots N_{Asto}$  **do**  
  **if**  $n > 1$  **then**  
     $\Theta_K = \Theta_{M^*}$ ;  $\mathfrak{F}_K = \mathfrak{F}_{M^*}$ ;  $K = K_0 - M^*$ ;  
  **for** *SmpIter*:  $k = 1 \dots K$  **do**  
    **if**  $\|\mathcal{K}_n^{md}\| \geq \bar{\mathcal{K}}tol$  **then**  
      Sample trajectory  $\theta_k \sim \mathcal{U}(\theta_{\min}, \theta_{\max})$ ;  
    **else**  
      Sample trajectory  $\theta_k \sim \mathcal{GP}(\mu_n^{md}, \mathcal{K}_n^{md})$ ;  
    Confine  $\theta_k$  in the motion constraints (47);  
     $\Theta_K \leftarrow \Theta_K \cup \theta_k$ ; Evaluate  $\mathcal{F}(\theta_k)$  by (14);  
    **if**  $\mathcal{F}_{obs}(\theta_k) \leq \mathcal{G}tol$  **then**  
      **return**  $\theta_k$  and  $\mathcal{GP}$  modified by (42).  
    **else**  
       $\mathfrak{F}_K = \mathfrak{F}_K \cup \mathcal{F}(\theta_k)$ ;  
 Extract the  $M^*$ -important samples with low cost from  $\Theta_K$  and construct a set  $\Theta_{M^*}$  and its  $\mathfrak{F}_{M^*}$ ;  
 Update the reward  $Q(\mu, \mathcal{K} | \mu_n^{md}, \mathcal{K}_n^{md})$  via EM;  
 /\* Learn the policy  $\mu, \mathcal{K}$  via AMA \*/  
 $\mu_n^{ag} = \mu_n^{md} + \beta_n^\mu \nabla \hat{\mathcal{R}}(\mu_n^{md})$ ;  
 $\mathcal{K}_n^{ag} = \mathcal{K}_n^{md} + \beta_n^\kappa \nabla \hat{\mathcal{R}}(\mathcal{K}_n^{md})$ ;  
 $\mu_n = \mu_{n-1} + \lambda_n^\mu \nabla \hat{\mathcal{R}}(\mu_n^{md})$ ;  
 $\mathcal{K}_n = \mathcal{K}_{n-1} + \lambda_n^\kappa \nabla \hat{\mathcal{R}}(\mathcal{K}_n^{md})$ ;  
 $\mu_{n+1}^{md} = (1 - \alpha_n^\mu) \mu_n^{ag} + \alpha_n^\mu \mu_n$ ;  
 $\mathcal{K}_{n+1}^{md} = (1 - \alpha_n^\kappa) \mathcal{K}_n^{ag} + \alpha_n^\kappa \mathcal{K}_n$ ;  
**if**  $\|\mathcal{K}_n^{md}\| \leq \bar{\mathcal{K}}tol$  or  $\exists \text{ eig}(\mathcal{K}_n^{md}) \leq 0$  or  $n \geq N_{Asto}$  **then**  
   $\theta = \text{argmin}_{\mu_n^{md} \cup \Theta_K} \mathcal{F}(\mu_n^{md}) \cup \mathfrak{F}_K$ ;  
  **if**  $\mathcal{F}(\theta) - \mathcal{F}(\mu_0) \leq \mathcal{F}(\mu_0) \cdot c\mathcal{F}tol$  **then**  
    **return**  $\theta$  and  $\mathcal{GP}$  modified by (42).  
  **else**  
    **return**  $\mu_0$  and  $\mathcal{GP}(\mu_0, \mathcal{K}_0)$ .  


---

like [62]. It contains the E-steps, which estimate the logarithm likelihood for reward gathering, and the M-steps that maximize the reward for policy updating.

1) *E-step*: Given the current policy  $\mathcal{GP}(\mu, \mathcal{K})$ , we determine the conditional distribution of  $\mathcal{F}_k = \mathcal{F}(\theta_k)$  (19) based on the Bayes theorem:

$$p_k = P(\mathcal{F}_k | \theta_k; \mu, \mathcal{K}) = \frac{e^{-\varpi \mathcal{F}_k} f(\theta_k; \mu, \mathcal{K})}{\sum_{k=1}^K e^{-\varpi \mathcal{F}_k} f(\theta_k; \mu, \mathcal{K})}, \quad (33)$$

where  $f(\theta_k; \mu, \mathcal{K})$  is the GP-defined probabilistic distribution function of a sample  $\theta_k$ .  $e^{-\varpi \mathcal{F}_k}$  denotes the latent probability<sup>7</sup> of a sample  $\theta_k$ , where the arithmetic operator [7]

$$\varpi \mathcal{F}_k = h_p \frac{\mathcal{F}_k - \min \mathfrak{F}_K}{\max \mathfrak{F}_K - \min \mathfrak{F}_K},$$

regulates the probabilistic distribution given  $\mathfrak{F}_K$  with a scalar  $h_p$  to control the variance.

<sup>7</sup>The word latent means the overall probability distribution  $p(\mathcal{F}[\theta])$  of  $\theta$  in the potential field  $\mathcal{F}$  is unmeasurable.

After gaining the probability  $P(\mathcal{F}_k | \theta_k; \mu, \mathcal{K})$  of (33), we get the reward  $\mathcal{R}$  of the policy  $\mathcal{GP}(\mu', \mathcal{K}')$  need to learn:

$$\begin{aligned} \mathcal{R}(\mu', \mathcal{K}' | \mu, \mathcal{K}) &= \mathbb{E}_{\mathcal{F}_K | \Theta_K; \mu, \mathcal{K}} [\log L(\mu', \mathcal{K}'; \Theta_K)] \\ &= \sum_{k=1}^K p_k \log L(\mu', \mathcal{K}'; \theta_k), \end{aligned} \quad (34)$$

where the function

$$L(\mu', \mathcal{K}'; \Theta_K) = \prod_{k=1}^K f(\theta_k; \mu', \mathcal{K}')$$

computes the likelihood of  $\mathcal{GP}(\mu', \mathcal{K}')$  given the sample set  $\Theta_K$ . The logarithm likelihood measures the sum of the negative Mahalanobis distance between the samples and the policy to optimize. So the reward  $\mathcal{R}$  will somewhat encourage the future policy getting close to the former. At the same time,  $\mathcal{R}$  will guide the future policy towards the samples with lower energy/cost through combining the conditional probability  $p_k$  informed by the environment.

2) *M-step*: After gaining the reward from E-step, M-step will prompt the policy learning. From Appendix B,  $\mathcal{R}$  could be expressed in a quadratic form. So we obtain the optimal  $\mu', \mathcal{K}'$  by searching for the maximum of  $\mathcal{R}$ :

$$\operatorname{argmax}_{\mu', \mathcal{K}'} \mathcal{R}(\mu', \mathcal{K}' | \mu, \mathcal{K}).$$

However, some useless information gathered by the samples with high cost could attach some extra computational resources for the EM-based  $\mathcal{GP}$ -adaptation and disturb the policy learning process. So we extract  $M^*$  important samples with low cost from  $\Theta_K$  like STOMP and only take  $\{\Theta_{M^*}, \mathcal{F}_{M^*}\}$  other than  $\{\Theta_K, \mathcal{F}_K\}$  into the calculation of the policy updating rules

$$\nabla \hat{\mathcal{R}}(\mu') = \hat{\mu} - \mu', \quad \nabla \hat{\mathcal{R}}(\mathcal{K}') = \hat{\mathcal{K}} - \mathcal{K}' \quad (35)$$

due to Appendix B<sup>8</sup>, where

$$\hat{\mu} = \frac{\sum_{m=1}^{M^*} p_m \theta_m}{\sum_{m=1}^{M^*} p_m}, \quad \hat{\mathcal{K}} = \frac{\sum_{m=1}^{M^*} p_m \cdot (\theta_m - \hat{\mu})^{\otimes 2}}{\sum_{m=1}^{M^*} p_m},$$

and  $[\cdot]^{\otimes 2} = [\cdot][\cdot]^T$  denotes the outer product of the two columnized values  $[\cdot]$ . If we use

$$\mu^M \leftarrow \mu + \nabla \hat{\mathcal{R}}(\mu), \quad \mathcal{K}^M \leftarrow \mathcal{K} + \nabla \hat{\mathcal{R}}(\mathcal{K})$$

to renew the policy, we can see  $\nabla \hat{\mathcal{R}}(\mu^M, \mathcal{K}^M) = 0$ , approaching the maximum reward with  $\Theta_{M^*}$ .

Now let us define  $\{\mu^K, \mathcal{K}^K\}$  as the learned policy informed by the whole set  $\Theta_K$  than the selected set  $\Theta_{M^*}$  and see how they perform differently from  $\{\mu^M, \mathcal{K}^M\}$  in the rewarding and learning process. Since (34)'s quadratic form indicates the convexity of the reward ascent problem, we directly get

$$\mathcal{R}(\mu^K, \mathcal{K}^K | \mu, \mathcal{K}) \geq \mathcal{R}(\mu^M, \mathcal{K}^M | \mu, \mathcal{K}),$$

which reveals that the  $M^*$ -selection method releases the strict  $\mathcal{R}$ -ascend. However, a phenomenon that

$$\mathbb{E}_{\mathcal{F}_K | \Theta_K; \mu, \mathcal{K}}(\mathcal{F}_K) \geq \mathbb{E}_{\mathcal{F}_{M^*} | \Theta_K; \mu, \mathcal{K}}(\mathcal{F}_{M^*})$$

<sup>8</sup> $\nabla \hat{\mathcal{R}}$  denotes a quasi-gradient than the gradient  $\nabla \mathcal{R}$ .

gives a rough intuition that  $\mathcal{F}(\mu^K) \geq \mathcal{F}(\mu^M)$ <sup>9</sup>. So we always use  $M^* \approx K/2$  to trade off between a better rewarding and a more efficient learning. That is also why the next part proposes the AMA method to improve ASTO's learning ability.

### B. Accelerated Moving Averaging

Moving averaging, shown in Figure 6, smoothes the stochastic learning process via the damped convolution to analyze the sampled data statistically in a time series. Recently, AMP [63] and iLSTF [64] employed the exponential moving averaging (EMA) method and introduced the forgetting coefficient to make a real-time prediction of a worker's movement. One of EMA's significant contributions is its high generalization capability via historical knowledge integration in a damped or forgetting way. This section adopts the fundamental theorem of EMA and proposes AMA for adaptive learning.

Since the end of Section VII-A2 indicates the release of the strict reward ascent could somewhat improve the learning procedure during the trajectory-functional interaction. We develop AMA based on AGD (Section III-A). It pretty much matches the rudimental theorem of AGD, which combines the historical information of momenta and releases the strict descent to approach the optimal convergence. So now let us first see how AMA performs EMA. According to (35) and Algorithm 3, we update  $\mu, \mathcal{K}$  with step  $\{\alpha_n^\mu, \alpha_n^\kappa, \beta_n^\mu, \beta_n^\kappa, \lambda_n^\mu, \lambda_n^\kappa\} = \{\alpha^\mu, \alpha^\kappa, \alpha^\mu, \alpha^\kappa, \alpha^\mu, \alpha^\kappa\}$ , then gain

$$\begin{aligned} \mu_{n+1}^{md} &= (1 - \alpha^\mu) \mu_n^{md} + \alpha^\mu \hat{\mu}_n, \\ \mathcal{K}_{n+1}^{md} &= (1 - \alpha^\kappa) \mathcal{K}_n^{md} + \alpha^\kappa \hat{\mathcal{K}}_n, \end{aligned} \quad (36)$$

which is the EMA method. It could release the reward ascent further, because the steps are selected as  $\alpha^\mu, \alpha^\kappa \in (0, 1)$ .

Adam [38], a popular stochastic optimization algorithm for deep learning, upgrades the EMA method with bias correction and improves logistic regression or neural network learning performance. So we reset  $\beta_n^\mu = (1 - \alpha^\mu)^n$ ,  $\beta_n^\kappa = (1 - \alpha^\kappa)^n$  and  $\lambda_n^\mu = 1 + \beta_n^\mu$ ,  $\lambda_n^\kappa = 1 + \beta_n^\kappa$  to correct the bias brought by EMA and gain

$$\begin{aligned} \mu_{n+1}^{md} &= \hat{\mu}_n + \alpha^\mu \sum_{i=1}^{n-1} \frac{(\hat{\mu}_i - \mu_i^{md}) - (\hat{\mu}_n - \mu_n^{md})}{(1 - \alpha^\mu)^{i-n}}, \\ \mathcal{K}_{n+1}^{md} &= \hat{\mathcal{K}}_n + \alpha^\kappa \sum_{i=1}^{n-1} \frac{(\hat{\mathcal{K}}_i - \mathcal{K}_i^{md}) - (\hat{\mathcal{K}}_n - \mathcal{K}_n^{md})}{(1 - \alpha^\kappa)^{i-n}}, \end{aligned} \quad (37)$$

according to Appendix C. The above quasi-Adam (qAdam)<sup>10</sup> method performs differently from EMA (36) since qAdam approximately transforms the step-size from  $\beta$  to  $(1 - \alpha)^n$  with  $\alpha \in (0, \frac{3-\sqrt{5}}{2})$ . It reveals that the maximum values  $\{\hat{\mu}_n, \hat{\mathcal{K}}_n\}$  make damped efforts from the initial to the final. To look inside the above methods deeper, we derive the convergence process of EMA (38) and qAdam (39) in each

<sup>9</sup>The word rough means the functional  $\mathcal{F}$  is nonconvex and the inequality that  $\mathcal{F}(\mu^K) \geq \mathcal{F}(\mu^M)$  cannot hold for  $\forall \mu^K, \mu^M$  satisfying the inequality relationship of  $\mathbb{E}_{\mathcal{F} | \Theta; \mu, \mathcal{K}}(\mathcal{F})$ .

<sup>10</sup>We call it qAdam because Adam [38] uses  $\frac{1}{1-(\alpha^\mu)^n}$  and  $\frac{1}{1-(\alpha^\kappa)^n}$  to correct (36)'s bias.

reward-step of *AstoIter* according to AGD in Section III-A and its ODE-interpretation in Section VI-A:

$$\min_{n=1,\dots,N} \|\nabla \mathcal{R}_n^{md}\|^2 \leq \frac{\mathcal{R}^* - \mathcal{R}_0}{\alpha(1 - \alpha\mathcal{L}_{\mathcal{R}})N}, \quad (38)$$

$$\mathcal{R}^* - \mathcal{R}_N^{ag} \leq \frac{1}{2}(1 - \alpha)^{N-1} \|\mathbf{gp}_0 - \mathbf{gp}^*\|^2, \quad (39)$$

where  $\mathbf{gp} = \{\boldsymbol{\mu}, \mathcal{K}\}$ ,  $\alpha = \min\{\alpha^\mu, \alpha^\kappa\}$ , and  $\mathcal{L}_{\mathcal{R}}$  is  $\mathcal{R}$ 's Lipschitz constant. Since ASTO sequentially gathers the environmental information and the whole learning process is strongly nonconvex and latent, we analyze the rewarding process informed by one single sampling or interaction to see how the above methods perform during the whole ASTO process. As a result, (39) shows the squared convergence rate of qAdam, and Section X-B2 validates that the damped process can correct the arbitrarily initialized  $\mathcal{GP}$  and stabilize the final steps. However, these advantages easily collapse due to the strongly nonconvex and unobservable RL process of ASTO. In this case, (37)'s residue brings more disturbances from the historical information forgotten exponentially than (36).

So another question about how to perform a damped process free of the prerequisites of convexity and observability comes up. Surprisingly, Corollary 1 provides a possible solution: we reset  $\alpha_n = \frac{2}{n+1}$ ,  $\beta = \mathcal{L}_Q^{-1}$ ,  $\lambda_n \sim \beta \cdot \mathcal{U}(1, 1 + \frac{\alpha_n}{4})$ . Then we gain the AMA process according to Appendix C:

$$\begin{aligned} \boldsymbol{\mu}_{n+1}^{md} &= \boldsymbol{\mu}_n^{md} + \alpha_n(\lambda_n - \beta)(\hat{\boldsymbol{\mu}}_n - \boldsymbol{\mu}_n^{md}) \\ &\quad + \alpha_{n-1}\Gamma_{n-1} \sum_{i=1} \Gamma_{i-1}^{-1}(\lambda_i - \beta)(\hat{\boldsymbol{\mu}}_i - \boldsymbol{\mu}_i^{md}), \\ \mathcal{K}_{n+1}^{md} &= \mathcal{K}_n^{md} + \alpha_n(\lambda_n - \beta)(\hat{\mathcal{K}}_n - \mathcal{K}_n^{md}) \\ &\quad + \alpha_{n-1}\Gamma_{n-1} \sum_{i=1} \Gamma_{i-1}^{-1}(\lambda_i - \beta)(\hat{\mathcal{K}}_i - \mathcal{K}_i^{md}). \end{aligned} \quad (40)$$

According to Corollary 1, we derive AMA's convergence:

$$\min_{k=1\dots N} \|\nabla \mathcal{R}_n^{md}\|^2 \leq \frac{25\mathcal{L}_{\mathcal{R}}(\mathcal{R}^* - \mathcal{R}_0)}{4(\sqrt{2} - 1)N}. \quad (41)$$

It shows a similar convergence process as EMA (38), and both of them could deal with some nonconvex cases. Unlike EMA using the constant forgetting factor  $\beta$ , AMA (63) utilizes the factor  $\alpha = \frac{2}{n+1}$  to damp the factor during RL like qAdam (37). Section X-B2 validates its high robustness and efficiency.

In practice, we set the maximum number  $N_{Asto} \sim \mathcal{U}(5, 15)$  of *AstoIter*, because ASTO depends on the initial steps deciding the searching area more than the upcoming steps for solution refinement mainly assigned to  $\mathcal{L}$ -reAGD of Section VI. Moreover, there are four terminate conditions for ASTO: (i) one of the sampled trajectories in  $\Theta_K$  is collision-free; (ii) the renewed GP-model is feasible; (iii) the maximum iteration time  $N_{Asto}$  is attached; (iv)  $\|\mathcal{K}_n^{md}\|$  converges to  $\underline{\mathcal{K}}_{tol}$ ; (v)  $\mathcal{K}_n^{md}$  is negative definite. When the condition (iii), (iv), or (v) is satisfied and the policy improvement misses the forecast, we will reject the updated GP model and return the original. Otherwise, we will accept and return the learned GP based on Section IV-B:

$$\begin{aligned} \boldsymbol{\mu} &= \boldsymbol{\mu}_0 + (\mathbf{C}\mathcal{K}_0)^T(\mathbf{C}\mathcal{K}_0\mathbf{C}^T + \mathcal{K}_\epsilon)^{-1}(\boldsymbol{\theta}^* - \mathbf{C}\boldsymbol{\mu}_0), \\ \mathcal{K} &= \mathcal{K}_0 - (\mathbf{C}\mathcal{K}_0)^T(\mathcal{K}_0 + \mathcal{K}_\epsilon)^{-1}\mathbf{C}\mathcal{K}_0, \end{aligned} \quad (42)$$

where  $\boldsymbol{\theta}^*$  is a learned policy when ASTO is terminated,  $\mathbf{C}$  is a system matrix defined by  $\mathfrak{H}$  (18), and  $\mathcal{K}_\epsilon$  decides the modification rate of the returning GP. After that, AGP-STO (Algorithm 2) will adopt the learned policy/trajectory and the modified GP to continue the MAP of trajectory.

## VIII. INCREMENTALLY OPTIMAL MOTION PLANNING VIA BAYES TREE INFERENCE

So far, we have introduced AGP-STO for the whole trajectory optimization. However, it always requires extra computation resources because of the high-dimension and step-size inconsistency in the first-order optimization case. Our former work [41] adopts the methodologies of iSAM2 [20] and iGPMP2 [19] and proposes reTraj-BTI for iSAGO to elevate the planning efficiency. However, iSAGO sometimes confronts the failure case where a significant gap exists between the feasible solution and the initial trajectory in the  $\mathcal{F}$ -field (Figure 3). TrajOpt [2] manually selects a few guidance waypoints and interpolates the support waypoints to gain the initial trajectory to moderate the above concerns.

Based on the manual selection in TrajOpt, this section proposes an incremental optimal motion planning (iOMP, Algorithm 4) method for time-continuous safety. iOMP first generates an initial trajectory consisting of a few guidance waypoints via linear interpolation between the start and goal point. Then it uses AGP-STO (Algorithm 2) iteratively in `iSAGO.reTrajIter()`.

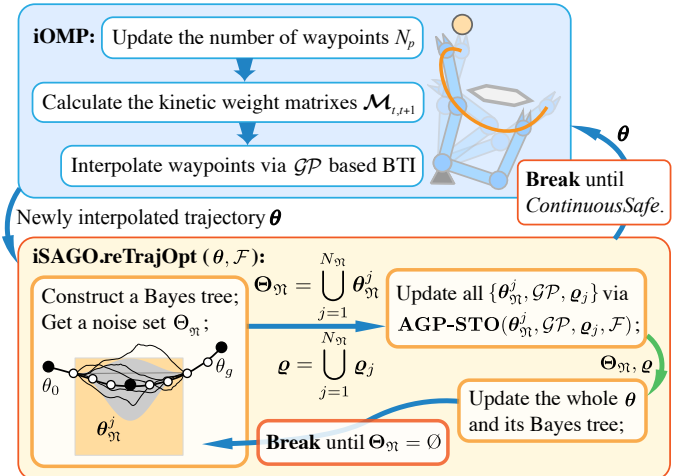


Fig. 7: A diagram shows how the incremental optimal motion planner (iOMP, Algorithm 4) interpolates the waypoints among the last support waypoints via the  $\mathcal{GP}$ -based Bayes tree inference (BTI). Moreover, the lower part of the diagram visualizes how `iSAGO.reTrajOpt` ( $\boldsymbol{\theta}, \mathcal{F}$ ) constructs a Bayes tree and gains a noise set  $\Theta_{ni}$  to incrementally plan an optimal trajectory via `AGPSTO` ( $\boldsymbol{\theta}_{ni}^j, \mathcal{GP}, \mathbf{q}_j, \mathcal{F}$ ).

In the outer loop *utiliter*, iOMP interpolates the support waypoints among the previously optimized trajectory via BTI. It means a proper allocation of the waypoints to interpolate can not only ensure the time-continuous safety but improve the efficiency of trajectory smoothing. So this section utilizes the kinetic energy  $\mathcal{F}_\kappa(t, t+1)$  between any adjacent waypoints  $\theta_t, \theta_{t+1}$  in the previous trajectory to determine the allocation. However, a direct calculation of the kinetic energy needs

**Algorithm 4: iOMP**


---

**Input:** Start point  $\theta_0$  and goal point  $\theta_g$ ;  
**1 Initialize:** number of waypoints  $N_p$ , time interval  $\Delta t$ ;  
**2 for** *itiler*:  $i = 1 \dots N_{itl}$  **do**  
**3**   Get  $\mathcal{GP}(\mu, \mathcal{K})$  via Bayes inference from  $\theta$ ;  
**4**   Renew  $\theta$  via (44)-interpolation;  
**5**   iSAGO.reTrajIter( $\theta, \mathcal{F}$ ):  
**6**      $k \leftarrow 1$ ; Get noisy set  $\Theta_{\mathcal{N}} = \bigcup_{j=1}^{N_{\mathcal{N}}} \theta_{\mathcal{N}}^j$ ;  
**7**     **if**  $\Theta_{\mathcal{N}} = \emptyset$  **or**  $k \geq N_{itf}$  **then break**;  
**8**     **for**  $j = 1, \dots, N_{\mathcal{N}}$  **do**  
**9**        $\{\theta_{\mathcal{N}}^j, \mathcal{GP}, \mathbf{q}_j\} \leftarrow \text{AGPSTO}(\theta_{\mathcal{N}}^j, \mathcal{GP}, \mathbf{q}_j, \mathcal{F})$   
       via **Algorithm 2**;  
**10**     Update the whole  $\theta$  and Bayesian tree;  
**11**     Eliminate the waypoints  $\theta \in \Theta_{\mathcal{N}}$  temporarily;  
**12**   **if** *ContinuousSafe* **then return**  $\theta$ .  
**13**   **else if**  $i \geq N_{itl}$  **then return** Failed.  
**14**   Update  $N_p \leftarrow \tau_{ip} \cdot N_p$ ,  $\Delta t \leftarrow \tau_{ip}^{-1} \cdot \Delta t$ ;

---

extensive computational resources for  $\int_t^{t+1} \frac{1}{2} \mathcal{I}(t) \dot{\theta}(t)^2 dt$ <sup>11</sup> because the inertia  $\mathcal{I}(t)$  of the whole robot is time-variant. So we first infer the mid-point  $\theta_{t+\frac{1}{2}}$  by GP (11), then approximate the kinetic energy via

$$\mathcal{F}_{\kappa}(t, t+1) = \frac{1}{2} \|\theta_t - \theta_{t+1}\|_{\mathcal{M}_{t,t+1}^{-1}}^2,$$

with the kinetic weight matrix

$$\mathcal{M}_{t,t+1} = \text{diag}(\mathcal{M}_i), i \in \mathcal{Q} = \{1, \dots, N_{\mathcal{Q}}\} \quad (43)$$

where  $\mathcal{Q}$  stores the indexes of robot's joints. With the gathered physical information, such as the inertia  $\mathbf{I}_{zz}$ , center of mass  $\mathbf{p}_{\text{CoM}}$ , and mass  $m$  of each rigid body, we approximate the inertia resisting joint- $i$  by

$$\mathcal{M}_i = \mathbf{I}_{zz}^i + \sum_{j \in \mathcal{B}_i} m_j \cdot \|\mathbf{T}_i^j(\theta_{t+\frac{1}{2}}) \cdot \mathbf{p}_{\text{CoM}}^j\|^2,$$

where set  $\mathcal{B}_i$  stores the indexes of the bodies actuated by joint- $i$ , and matrix  $\mathbf{T}_i^j$  uses the midway state  $\theta_{t+\frac{1}{2}}$  to transform body- $j$  from joint- $i$  in  $\text{SE}(3)$ . After that, we allocate the number of interpolation waypoints between  $\theta_t$  and  $\theta_{t+1}$  by

$$N_p^{t,t+1} = \text{round} \left( N_p \cdot \frac{\mathcal{F}_{\kappa}(t, t+1)}{\sum_{t \in [t_0, t_g]} \mathcal{F}_{\kappa}(t, t+1)} \right). \quad (44)$$

It means that there are more waypoints in the interval with relatively higher kinetic energy.

In the inner loop `iSAGO.reTrajIter( $\theta, \mathcal{F}$ )` [41], iOMP decomposes the whole trajectory optimization into a series of sub-replanning problems to improve the computation efficiency and success rate. This iteration first gains the noisy set  $\Theta_{\mathcal{N}}$  consisted of  $N_{\mathcal{N}}$  sub-trajectories  $\theta_{\mathcal{N}}$  with significant Bayes tree factor. Then it uses AGP-STO to optimize  $\theta_{\mathcal{N}}$  with its corresponding penalty factor  $\mathbf{q}$  incrementally and updates the Bayes tree informed by the GP and constraints  $\mathcal{G}$ . When all the significant factors are flattened (i.e.,  $\Theta_{\mathcal{N}} = \emptyset$ ), it will

<sup>11</sup> $\dot{\theta}(t)$  denotes the higher derivation of the state  $\theta$  with respect to time  $t$ .

terminate. To prevent the informational leakage of  $\mathcal{G}$ , iOMP exponentially expands the number  $N_p$  of the waypoints to interpolate until the trajectory is *ContinuousSafe*.

## IX. IMPLEMENTATION DETAILS

## A. GP prior

This paper utilizes the LTV-SDE with constant velocity (i.e., zero acceleration) for the GP prior construction through (6) according to [3]:

$$\mathbf{A}(t) = \begin{bmatrix} \mathbf{0} & \mathbf{I} \\ \mathbf{0} & \mathbf{0} \end{bmatrix}, \mathbf{u}(t) = \mathbf{0}, \mathbf{F}(t) = \begin{bmatrix} \mathbf{0} \\ \mathbf{I} \end{bmatrix},$$

and given  $\Delta t_i = t_{i+1} - t_i$ ,

$$\Phi(t, s) = \begin{bmatrix} \mathbf{I} & (t-s)\mathbf{I} \\ \mathbf{0} & \mathbf{I} \end{bmatrix}, \mathbf{Q}_{t,t+1} = \begin{bmatrix} \frac{1}{3}\Delta t^3 & \frac{1}{2}\Delta t^2 \\ \frac{1}{2}\Delta t^2 & \Delta t \end{bmatrix} \otimes \mathbf{Q}_c. \quad (45)$$

In practice, the ASTO method in Section VII only samples the trajectories consisted of position states under the zero velocity assumption and utilizes the discretization method  $\frac{x(t_{i+1}) - x(t_i)}{\Delta t}$  rather than the analytic method requiring Jacobian to calculate  $\dot{x}(t_i)$  more efficiently for  $\mathcal{F}$ -estimation.

## B. Collision-cost function

Some previous works [1], [2], [13], [18] are almost first-order continuously differentiable. It always requires extra  $\mathcal{L}_{\mathcal{F}}$ -estimation steps in Section VI-B because of the second-order discontinuity. Our work designs a collision cost function with the forth-order polynomial piecewise form:

$$c(\mathcal{D}) = \begin{cases} \frac{\epsilon}{2} - \mathcal{D} & \text{if } \mathcal{D} < 0 \\ \frac{1}{\epsilon^2}(\epsilon - \mathcal{D})^3 - \frac{1}{2\epsilon^3}(\epsilon - \mathcal{D})^4 & \text{if } 0 \leq \mathcal{D} \leq \epsilon \\ 0 & \text{otherwise,} \end{cases} \quad (46)$$

where  $\mathcal{D}(x) : \mathbb{R}^3 \rightarrow \mathbb{R}$  maps the CCB-position in  $\text{SE}(3)$  into the singed distance, and  $x(\theta, S_i) : \mathbb{R}^{N_{\theta}} \rightarrow \mathbb{R}^3$  maps the joint states into the position of bounding box  $S_i \in \mathcal{B}$ . The collision cost function above is a quartic polynomial and second continuously differentiable. Figure 5 visualizes an example of the collision field defined by (46), while Figure 8 visualizes three types of robot represented by a series of CCBs in three planning scenarios.

## C. Motion constraints

As for the motion constraints, we uses the same cost function as [3]:

$$c(\theta_i^d) = \begin{cases} -\theta_i^d + \theta_{\min}^d - \epsilon & \text{if } \theta_i^d < \theta_{\min}^d + \epsilon_d \\ \theta_i^d - \theta_{\max}^d + \epsilon & \text{if } \theta_i^d > \theta_{\max}^d - \epsilon_d \\ 0 & \text{otherwise,} \end{cases} \quad (47)$$

where  $\theta_i^d$  is the  $d^{\text{th}}$  joint state at time  $i$ ,  $\theta_{\min}^d$  and  $\theta_{\max}^d$  are the lower and upper joint motion limits respectively, and  $\epsilon_d$  aims to bound the joint states within a safe area.

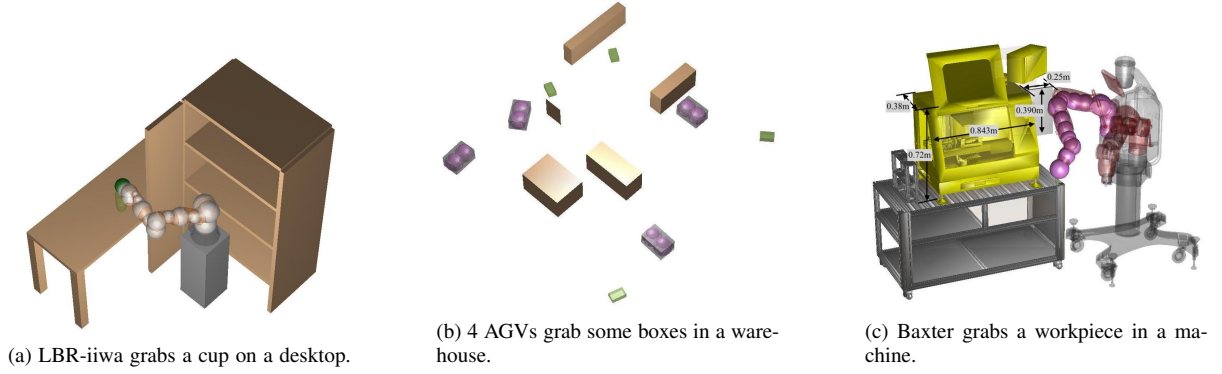
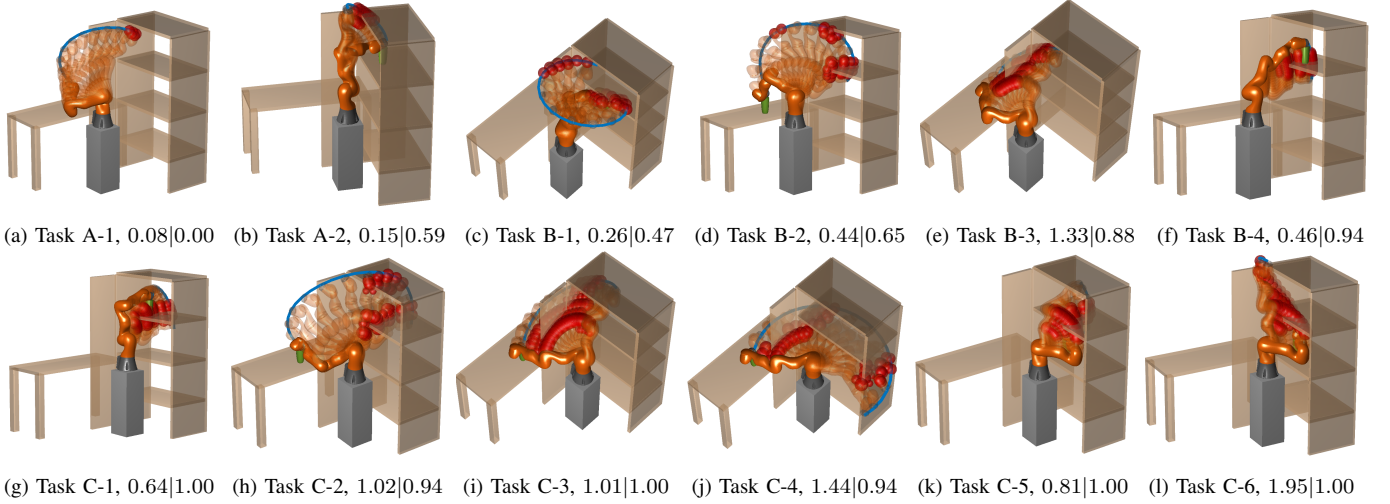


Fig. 8: The geometrically connected collision check balls (CCBs) assemble the robot.

Fig. 9: The initial trajectory with the red boxes in collision demonstrates the task categorized in Table II. Note that *Task A-1*,  $0.04|0.15$  means task 1 of class A, whose  $\bar{\mathcal{F}}|\mathcal{S} = 0.04|0.15$  due to (49).

## X. EVALUATION

We evaluate iAGP-STO on multi-AGV collaboration, LBR-iiwa manipulation, and rethink-Baxter assistance with 10, 50, and 5 planning problems, respectively, in three scenarios (Figure 8). Our experiment first tunes their key parameters on LBR-iiwa in Section X-B to show the contribution of each part of iAGP-STO. It then benchmarks iAGP-STO against  $\mathcal{L}$ -reAGD, AGP-STO, TrajOpt, GPMP2, CHOMP, RRT-Connect, and STOMP for cross-validation in Section X-D. After that, Section X-E and Section X-F implement iAGP-STO on multi-AGV and rethink-Baxter.

### A. Setup for planning benchmark

Our experiment compares iAGP-STO with the numerical planners: CHOMP [1], TrajOpt [2], [13], and GPMP2 [3], as well as the sampling planners: RRT-Connect [5] and STOMP [7]. Since all of our experiments are evaluated in MATLAB, we encode GPMP2 with option `GPMP2_BUILD_MATLAB_TOOLBOX = ON` to utilize `BatchTrajOptimize3Darm` and use `manipulator-RRT`<sup>12</sup> with `MaxConnectionDistance =  $\frac{\|\theta_g - \theta_0\|}{N}$`  for

RRT-Connect. Since TrajOpt internally uses Gurobi for the trust-region method, our benchmark uses `fmincon`<sup>13</sup> with `optimoptions('fmincon','Algorithm','trust-region-reflective','SpecifyObjectiveGradient',true)`, specifying `ObjectiveGradient` analytically and `Aeq` as a matrix consisted of the active constraint gradients calculated via numerical differentiation like TrajOpt. As for CHOMP, our benchmark defines an `hmcSampler` object with logarithm *pdf* (`logpdf`) defined by (14) and uses `hmcSampler.drawSamples` for HMC<sup>14</sup>. The above MATLAB functions are encoded into C-MEX files, because iAGP-STO is developed on GPMP2 and GTSAM [65] and encoded via CMake. As for STOMP, we only use ASTO with  $\{\alpha_n^\mu, \alpha_n^\kappa, \beta_n^\mu, \beta_n^\kappa, \lambda_n^\mu, \lambda_n^\kappa\} = \{\mathcal{K}_n^{md}, \mathbf{I}, \mathbf{I}, \mathbf{0}, \mathbf{0}, \mathbf{0}\}$  for the sequential resampling and updating of noise-trajectory. Furthermore, all benchmarks are run on a single thread of 2.3 GHz Intel Core i9 with 16 GB 2667 MHz DDR4.

Since a large number of waypoints could prevent the leakage of collision information  $\mathcal{G}$  while requires a large amount of

<sup>13</sup>See more at [https://www.mathworks.com/help/optim/ug/minimization-with-equality-constraints.html?searchHighlight=trust-region-reflective&s\\_tid=srchtitle\\_trust-region-reflective\\_5](https://www.mathworks.com/help/optim/ug/minimization-with-equality-constraints.html?searchHighlight=trust-region-reflective&s_tid=srchtitle_trust-region-reflective_5).

<sup>14</sup>See more at <https://www.mathworks.com/help/stats/hamiltoniansampler.drawsamples.html>.

<sup>12</sup>See more at <https://www.mathworks.com/help/robotics/ref/manipulatorrrt.html>.

computational resource, our benchmark first selects the initial number of waypoints

$$N_p = \begin{cases} 1 \text{ or } 2 & \text{if } 0 < \frac{\|\theta_g - \theta_0\|}{\|\theta_{\max} - \theta_{\min}\|} \leq \frac{1}{2} \\ 3 \text{ or } 4 & \text{if } \frac{1}{3} < \frac{\|\theta_g - \theta_0\|}{\|\theta_{\max} - \theta_{\min}\|} \leq 1, \end{cases} \quad (48)$$

depending on the length  $\|\theta_g - \theta_0\|$  between the initial waypoint  $\theta_0$  and goal waypoint  $\theta_g$ . The overlapping among different  $N_p$  exists because some long feasible trajectories have a small value of  $\|\theta_g - \theta_0\|$ . Then we generate the initial trajectory consisting of  $N_p$  support waypoints with 8 interval states through Bayes inference [3] according to Section IX-A rather than linear interpolation [1], [2], [7], [13]. After that, ITI plans an optimal motion incrementally until the trajectory is *ContinuousSafe*. According to a large amount of experiments, the final feasible trajectory contains 12 to 20 support waypoints with 8 interval waypoints. In this way, our benchmark sets 16 support states with 8 interval states (152 states in total) for GPMP2, 152 support states for CHOMP and STOMP, 76 support states for TrajOpt, and  $\text{MaxConnectionDistance} = \frac{\|\theta_g - \theta_0\|}{76}$  for RRT-connect. Except for the above settings, our benchmark uses the default settings of other planners.

To show the competence of iAGP-STO in solving OMP problems, we conduct 50 experiments with different start and goal states inside the desktop and shelf (Figure 8a). The experiments are classified into 3 categories (A, B, C). Planning difficulty increases with the stuck cases [41] of initial trajectory because the feasible T-space shrinks when the surrounding obstacles tighten and restrain the robot's motion. For an appropriate classification, we first estimate

$$\bar{\mathcal{F}} = \mathcal{F}(\theta)/N_p, \quad \mathfrak{S} = \max_{t=1 \dots N_p} N_{\mathfrak{S}}^t/17, \quad (49)$$

where  $N_{\mathfrak{S}}^t$  denotes the number of stuck cases on  $t$ -th support waypoint<sup>15</sup>. Then we classify the problems according to Table II, and generate 3 tasks for class A, 5 tasks for class

TABLE II: Planning Problem Classification

|                     | Class A   | Class B      | Class C            |
|---------------------|-----------|--------------|--------------------|
| $\bar{\mathcal{F}}$ | (0, 0.18] | (0.18, 1.40) | (0.60, $+\infty$ ) |
| $\mathfrak{S}$      | [0, 0.53] | (0.41, 0.88] | (0.88, 1.00]       |

B and 8 tasks for class C. Figure 9 shows that each problem type is a specific grabbing task with a previously specified goal requirement and contains 3 or 4 sub-problems with a random collision-free initial state and preset goal state. Moreover, we can directly observe that the number of collision cases denoted by the red boxes in Figure 9 increases from class A to class C. Since iAGP-STO, RRT-connect, STOMP, and CHOMP utilize the sampling method to search for feasible trajectory, we conduct 5 repeated trials for each problem to gain reliable experiment results.

### B. Key parameter tuning

Section V shows how AGP-STO (Algorithm 2) infers a collision-free trajectory from  $\mathcal{GP}$  prior and environmental

information  $\mathcal{G}$  via integrating  $\mathcal{L}$ -reAGD and ASTO. So this section shows how their performance varies in corresponding to parameter variation in Section X-B1 and Section X-B2.

1)  *$\mathcal{L}$ -reAGD parameter*: Since  $\mathcal{L}$ -reAGD adaptively restarts the AGD process with the reestimated  $\mathcal{L}_{\mathcal{F}}$ , this section tunes  $\{\vartheta_1, \vartheta_2\}$  around  $\{2, 0.25\}$  according to Corollary 1 and [11], and compares it with the AGD with a constant  $\mathcal{L}_{\mathcal{F}}=1e2$  (AGD-1e2). Since they are designed for the semi-convex problem, we select 10 problems from class A & B for the tuning experiment and analyze the results statistically.

The results of tuning experiments (Figure 10) show that  $\vartheta_1$  mainly determines the overall performance of  $\mathcal{L}$ -reAGD. The process tends to converge to 0 when  $\vartheta_1$  is nearby 2.000 while drops into the local minimum otherwise. So Figure 10 details how  $\mathcal{L}$ -reAGD performs differently when  $\vartheta_1 \in [1.000, 5.567]$  and  $\vartheta_2 \in [0.000, 0.875]$  especially  $\vartheta_1 \in \{2.000, 2.282\}$  and shows the best performance when  $\{\vartheta_1, \vartheta_2\} = \{2.000, 0.250\}$ . Table III indicates that a larger  $\vartheta_2$  determining the accelerated step of AGD can improve the convergence rate by 10%-70% and the success rate by 10%-150%. Moreover, each sub-figure of Figure 10 illustrates 10 different  $\mathcal{L}$ -reAGDs denoted by the solid lines and 10 different AGDs denoted by the dash lines and uses the purple and pink area to show their 95% confidence interval of expectation under a specific  $\{\vartheta_1, \vartheta_2\}$ . Moreover, Table III validates that the  $\mathcal{L}$ -restart significantly improves computational efficiency by 95% and robustness by 30%-80% compared to AGD-1e2.

TABLE III: Tuning  $\vartheta_1$  and  $\vartheta_2$  of  $\mathcal{L}$ -reAGD

| $\frac{(\%)(s)}{\vartheta_2} \backslash \vartheta_1$ | 1.000   | 1.414   | 2.000           | 2.828          | 4.000   | 5.657   |
|--|---------|---------|-----------------|----------------|---------|---------|
| 0.000  | 50 1.54 | 50 2.03 | 40 2.51         | 40 2.65        | 30 2.98 | 20 3.13 |
| 0.125  | —       | 60 2.16 | 70 3.03         | <b>90 4.87</b> | 30 2.44 | 20 2.98 |
| 0.250  | —       | 70 1.89 | <b>100 0.98</b> | 80 3.27        | 40 2.25 | 30 2.78 |
| 0.375  | —       | —       | <b>90 1.49</b>  | 80 4.26        | 40 1.92 | 20 2.45 |
| 0.500  | —       | —       | 80 1.76         | 80 2.03        | 30 1.77 | 20 2.89 |
| 0.625  | —       | —       | —               | 80 1.88        | 30 1.89 | 20 2.56 |
| 0.875  | —       | —       | —               | 80 1.67        | 40 1.73 | 40 2.43 |
| AGD-1e2  | 20 46.2 | 20 49.3 | 20 50.3         | 20 55.0        | 20 55.0 | 20 55.0 |

2) *ASTO parameter*: According to Section VII and Algorithm 3, the prior GP knowledge, the number of samples, and the Lipschitz constant  $\mathcal{L}_{\mathcal{R}}$  of the rewards  $\mathcal{R}$  highly affect the learning process of ASTO. Since the covariance matrix  $\mathcal{K}$ , calculated by  $\Delta t$  (45), mainly determines the searching space, our experiment first tunes  $\Delta t$  around 1 and keeps  $K|M^* = 12|6$  constant. Then our experiment tunes  $K|M^*$  around  $12|6$  and keeps  $\Delta t = 4$  constant to show how the number of samples affects the learning process. Moreover, the above experiments both tune  $\mathcal{L}_{\mathcal{Q}}$  around 10 and compare AMA, EMA, and qAdam, because AMA determined by  $\mathcal{L}_{\mathcal{R}}$  refines the learning process informed by the reward  $\mathcal{R}$  and the selected samples  $\Theta_{M^*}$ . Moreover, we set  $\{\alpha^\mu, \alpha^\kappa\}$  as  $\{0.1, 0.1\}$  or  $\{0.9, 0.9\}$  to compare AMA with EMA-0.1/EMA-0.9 and qAdam-0.1/qAdam-0.9 according to (36) and (37), respectively. All of the tuning tests run the whole iAGP-STO to solve 25 problems of class C, where  $\mathcal{L}$ -reAGD's parameters are set following Table V.

<sup>15</sup>Since our benchmark sets 8 interval waypoints for continuous safety, it is reasonable to apply  $2 \times 8 + 1 = 17$  for stuck-case estimation.

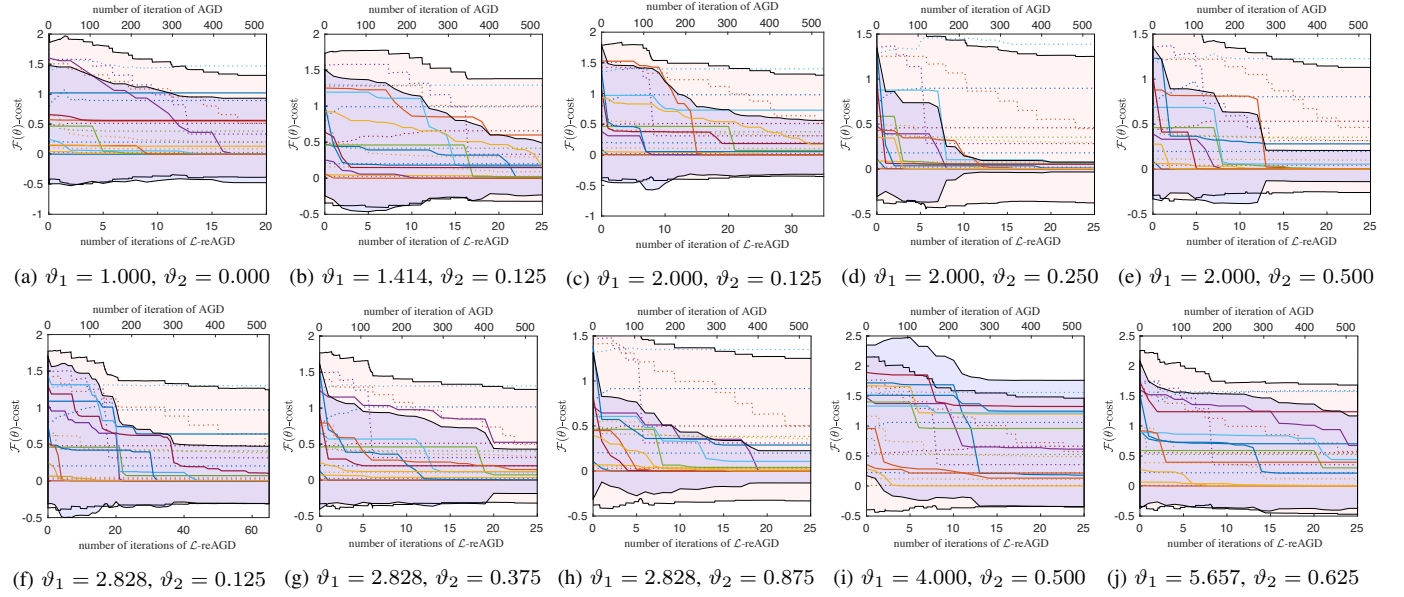


Fig. 10: A figure shows how  $\mathcal{L}$ -reAGD and AGD perform under variant key parameters during the tuning experiments. The solid and dash lines denote the processes of  $\mathcal{L}$ -reAGD and AGD, while the purple and pink areas denote the 95% confidence interval of their expectation, respectively.

Table IV.A shows that a small  $\mathcal{K}$  with a small  $\Delta t$  tightens the searching space around the prior mean value  $\mu$ . It reduces the success rate '(%)' by 55% and increases the average computation time '(s)' by 200% for the extra sampling and numerical process. On the contrary, a large  $\mathcal{K}$  with the over-released searching space also lowers the computational efficiency by 25% and the algorithmic robustness by 10%. Table IV.B indicates that a more significant number of samplings improves the success rate of ASTO by 10% while increasing the computational cost by 300% caused by the functional estimation of the extra samples. They both validate our intuition (the end of Section VII-A2) that a proper release of strict rewarding ascent can improve the learning ability. That is because a larger  $\mathcal{L}_{\mathcal{R}}$  meaning more leakage of rewarding strengthens the learning ability of ASTO and improves the success rate by 50% and computation time by 35%. Moreover, they both show AMA's higher robustness (20%) and efficiency (40%) compared to EM and qAdam.

### C. Parameter setting

Besides the above settings, we set  $\epsilon = 0.05$ ,  $\epsilon_d = 1e-2$  and other parameters according to Table V.

### D. Results analysis

This section shows the benchmark results of all OMP problems (class A, B, C) specified by Section X-A and Table II in Table VI.A-VI.B. Besides, Figure 11 randomly draws the planning results of the problems in class B and C.

Table VI.A shows that iAGP-STO could gain the optimal trajectory in the second- lowest computational time and highest success rate. Because the iAGP-STO only utilizes the gradient information without the Hessian calculation adopted by GPMP and makes 5% improvement. Besides, the fair judging of *MinAprch* successfully integrates ASTO to place the trajectory in the feasible space with a few resampling processes.

It makes 60%, 65%, and 80% improvement of efficiency compared to CHOMP-HMC, STOMP, and RRT-Connect. That is because STOMP needs plenty of time for the iterative processes containing resampling and simulation, though there is no need for gradient calculation. The vast searching space of RRT-connect easily neglects the subspace near the initial trajectory. TrajOpt shows 70% better convergence rate while 10% lower success rate for the convex constrained problems in the trust-region method. As for CHOMP-HMC, though HMC costs 10%-60% less time than STOMP and RRT-connect, the iterative alternation between the Hamiltonian simulation and the Monte Carlo sampling take up extra computation resource. Besides, CHOMP (without HMC) saves 50% more computation resources while reducing the success rate by 10% than CHOMP-HMC and validates  $\mathcal{L}$ -reAGD's priority over the leapfrog method in success rate by 5%.

Table VI.B shows that iAGP-STO gains the highest success rate compared to the other planners' thanks to our numerical and sampling methods integration. Because ASTO performs the resampling process iteratively rather than the iterative alternation between numerical optimization and single resampling process, iAGP-STO can find a feasible subspace more reliably (about 200%) and save 65% computation time in comparison to CHOMP. Moreover, the AMA method of ASTO and appropriate selection of  $\mathcal{K}$  elevate the success rate by 250% and save 65% computation resources compared to STOMP. Although RRT-connect adopts the bidirectional searching method and is provably probabilistically complete, it occupies 50% more computation resources to store the searching tree and check collision facing the narrow feasible space. Though HMC samples the momentum and finds the Hamiltonian minimum numerically, CHOMP performs badly when nonconvex infeasible sets surround the initial trajectory. As for GPMP and TrajOpt, the LM and trust-region method help them approach the local minima rapidly. However, whether the final optimized

Table IV.A Tuning  $\Delta t$  and  $\mathcal{L}_{\mathcal{R}}$  of ASTO

| $\begin{smallmatrix} (\%)(s) \\ \Delta t \end{smallmatrix} \backslash \mathcal{L}_{\mathcal{R}}$ | 100      | 10.0            | 4.00     | 2.00     | 1.25     | EMA-0.1  | EMA-0.9  | qAdam-0.1 | qAdam-0.9 |
|--|----------|-----------------|----------|----------|----------|----------|----------|-----------|-----------|
| 0.25   | 36 8.389 | 40 7.557        | 44 6.313 | 44 5.988 | 36 6.274 | 28 10.93 | 32 9.598 | 40 5.235  | 36 6.231  |
| 1.00   | 52 4.124 | 72 3.382        | 68 3.434 | 68 3.513 | 48 4.012 | 56 4.817 | 60 3.981 | 64 4.845  | 60 4.234  |
| 2.00   | 64 3.912 | 80 2.899        | 84 2.982 | 84 3.123 | 64 3.233 | 68 3.235 | 80 2.678 | 76 4.456  | 72 4.617  |
| 4.00   | 76 3.329 | <b>92 2.442</b> | 88 2.763 | 76 3.892 | 60 3.723 | 76 3.238 | 76 3.557 | 84 4.744  | 76 3.554  |
| 8.00   | 68 3.981 | 84 2.983        | 80 3.201 | 76 3.456 | 76 3.211 | 64 4.099 | 68 3.778 | 80 3.283  | 56 3.202  |

Table IV.B Tuning  $K|M^*$  and  $\mathcal{L}_{\mathcal{R}}$  of ASTO

| $\begin{smallmatrix} (\%)(s) \\ K M^* \end{smallmatrix} \backslash \mathcal{L}_{\mathcal{R}}$ | 100      | 10.0            | 4.00             | 2.00     | 1.25     | EMA-0.1  | EMA-0.9  | qAdam-0.1 | qAdam-0.9 |
|---|----------|-----------------|------------------|----------|----------|----------|----------|-----------|-----------|
| 8 4   | 76 2.991 | 88 1.722        | 84  <b>1.709</b> | 64 2.923 | 54 2.679 | 72 2.255 | 52 2.371 | 88 2.760  | 48 2.364  |
| 12 6  | 76 3.329 | 92 2.442        | 88 2.763         | 76 3.892 | 60 3.723 | 76 3.072 | 76 3.557 | 84 4.774  | 76 3.554  |
| 18 9  | 76 6.317 | 92 3.553        | 84 4.083         | 68 7.328 | 52 5.384 | 76 4.678 | 68 5.078 | 92 3.678  | 60 4.289  |
| 36 18   | 84 13.92 | <b>96 7.125</b> | 92 8.032         | 80 11.40 | 60 10.25 | 80 10.40 | 84 9.323 | 92 5.981  | 72 6.889  |

TABLE V: Parameter Setting

| algo.                | para.                           | meaning  | value  |
|----------------------|---------------------------------|--|--|
| iOMP                 | $\Delta t$                      | initial time interval                              | 4.0  |
|                      | $Q_c$                           | power-spectral density matrix                      | <b>I</b>   |
|                      | $\tau_{ip}$                     | interpolation scaling factor                       | 2  |
| AGP-STO              | $\varrho$                       | initial Lagrangian factor                          | <b>0.01</b>                                      |
|                      | $\mathcal{F}_{tol}$             | convergence of functional cost                     | 1e-5   |
|                      | $\theta_{tol}$                  | convergence of gradient norm                       | 1e-4   |
|                      | $\mathcal{G}_{tol}$             | collision cost tolerance                           | 1e-4   |
|                      | $\kappa$                        | penalty scaling factor                             | 0.4  |
| $\mathcal{L}$ -reAGD | $c_{low}$                       | factor of lower predicted reduction                | 1.25   |
|                      | $c_{up}$                        | factor of upper predicted reduction                | 0.15   |
|                      | $\vartheta_1$                   | scaling factor of $\beta_k$                        | 2  |
|                      | $\vartheta_2$                   | scaling factor of $\lambda_k$                      | 0.25   |
|                      | $\phi_{tol}$                    | slope tolerance of $\phi$                          | -0.1   |
|                      | $\mathcal{L}_{tol}$             | expanding tolerance of $\mathcal{L}_{\mathcal{F}}$ | 1e2  |
| ASTO                 | $K M^*$                         | number of overall selected samples                 | 12 6   |
|                      | $\mathcal{L}_{\mathcal{R}}$     | Lipschitz constant of reward $\mathcal{R}$         | 10   |
|                      | $c_{\mathcal{F}tol}$            | improvement rate tolerance                         | 0%   |
|                      | $\bar{\mathcal{K}}_{tol}$       | upper tolerance of $\mathcal{K}$ -norm             | $\frac{\ \theta_{max} - \theta_{min}\ ^2}{1.25}$ |
|                      | $\underline{\mathcal{K}}_{tol}$ | lower tolerance of $\mathcal{K}$ -norm             | 1e-2   |
|                      | $N_{Asto}$                      | maximum number of $AstoIter$                       | $\mathcal{U}(5, 15)$                             |

trajectory is feasible depends on whether the initial point is in the convex neighbor of the global minimum.

Table VI.A & VI.B both show that iOMP utilized by iAGP-STO improves the computation efficiency by 25%-50% compared to AGP-STO, which benefited from the incremental method. Moreover, the integration of ASTO and  $\mathcal{L}$ -reAGD elevates the success rate by 600% and only takes 50% more computation resources for trajectory resampling and numerical refinement than  $\mathcal{L}$ -reAGD.

### E. Multiple AGV collaboration

This part will illustrate how a multi-AGV robotic system with 12 DoFs reallocates 4 AGVs to safely grab and load 4 boxes in a warehouse containing obstacles. The red area of initial trajectories in Figures 12a-12c shows the interference between multiple AGVs and obstacles when AGVs transfer the boxes to different locations. In this way, our implementation sets  $\epsilon = 0.25$  for collision-check considering the safety of hybrid motion, initial penalty factor  $\varrho = 0.03125$ , and the others according to Table V. To further test iAGP-STO's

solvability, we conduct 5 repeated trials for each task given an initial state and goal constraint.

Figure 12b shows that 4 AGVs grab the boxes located at the safe places of the warehouse from the default state, bypassing the crossroad surrounded by some obstacles. While Figure 12d shows they load the boxes to other randomly generated locations, avoiding self-collision. The 100% success rate with 4.537s average time shows the high reliability and efficiency of iAGP-STO.

### F. rethink-Baxter assistance

This part will illustrate how a rethink-Baxter robot with 7 DoFs executes a collision-free motion to grab and load an aluminum workpiece in a computer numerical control (CNC) machine with a highly compact structure. The red area on initial trajectories of the tasks in Figure 13 shows the interference between the arm and the shelf when AUBO-i5 is transferring the workpiece between different cells. In this way, our implementation sets  $\epsilon = 0.025$  for collision-check considering the narrow space of the CNC machine,  $\Delta t = 2$  because of the narrower feasible motion region, and the others according to Table V. To further test iAGP-STO's solvability, we conduct 5 repeated trials for each task.

Figure 14a shows that Baxter first waves its front arm to avoid the open door and then worms itself to grab a workpiece inside the CNC machine from the default state. While Figure 14b shows that it loads the workpiece from one station to another outside the CNC machine, bypassing the opening door. The 90% success rate and 2.072s average time show the high reliability and efficiency of iAGP-STO. Moreover, we experiment in a real industrial environment to validate the above simulation in Figure 13, and their results are shown in Figure 14c-14d.

## XI. DISCUSSION

AGP-STO adopts GPMP to formulate the OMP problem and integrates the numerical and sampling method for highly reliable and efficient planning in the hazardous W-space.

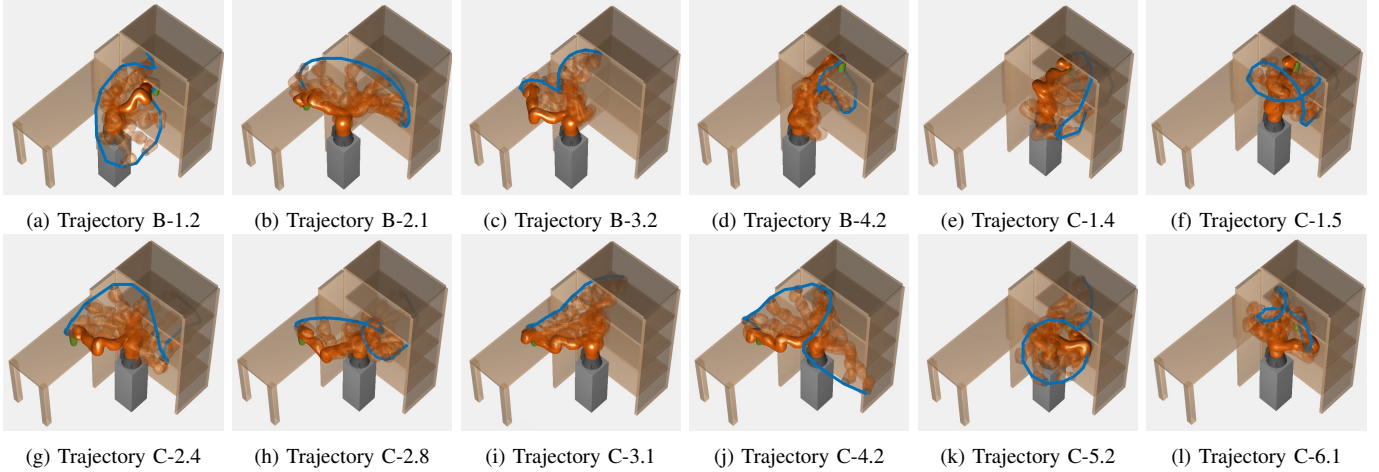
GPMP mainly concentrates on generalizing the collision-free OMP problem based on CHOMP and TrajOpt. However,

Table VI.A Results of 10 class **A** and 15 class **B** planning problems (with 5 repeated trials for each) on LBR-iiwa with 7-DoF.

|                   | $\mathcal{L}$ -reAGD | AGP-STO    | iAGP-STO   | TrajOpt-78   | GPMP-16 | CHOMP | CHOMP-HMC | STOMP | RRT-Connect |
|-------------------|----------------------|------------|------------|--------------|---------|-------|-----------|-------|-------------|
| Success (%)       | 84.8                 | <b>100</b> | <b>100</b> | 88           | 95.2    | 81.6  | 93.6      | 96.8  | <b>100</b>  |
| Avg. Time (s)     | 1.318                | 3.047      | 1.718      | <b>0.513</b> | 1.771   | 2.219 | 4.503     | 5.101 | 11.00       |
| Std-Dev. Time (s) | 0.735                | 1.048      | 0.139      | 0.050        | 0.325   | 0.412 | 0.899     | 3.233 | 4.728       |

Table VI.B Results of 25 class **C** planning problems (with 5 repeated trials for each) on LBR-iiwa with 7-DoF.

|                   | $\mathcal{L}$ -reAGD | AGP-STO | iAGP-STO    | TrajOpt-78   | GPMP2-16 | CHOMP | CHOMP-HMC | STOMP | RRT-Connect |
|-------------------|----------------------|---------|-------------|--------------|----------|-------|-----------|-------|-------------|
| Suc. Rate (%)     | 12.8                 | 87.2    | <b>91.2</b> | 8.8          | 11.2     | 8.0   | 30.4      | 24.8  | 72.8        |
| Avg. Time (s)     | 1.622                | 4.284   | 2.442       | <b>1.163</b> | 2.587    | 3.584 | 7.238     | 8.176 | 17.08       |
| Std-Dev. Time (s) | 0.735                | 1.048   | 0.419       | 0.104        | 1.345    | 0.577 | 1.322     | 5.364 | 2.726       |

Fig. 11: A figure shows the randomly selected results of iAGP-STO in class B and C, where the randomly selected goal states satisfy the same goal requirement in one task. Note that  $X3$  in *Trajectory  $X1$ - $X2$ . $X3$*  means a single problem  $X3$  in task  $X2$  categorized into class  $X1$ .

AGP-STO directly adopts the GPMP's formulation and focuses on approaching the global optima more reliably and efficiently. To infer a trajectory by MAP given the information of GP prior and obstacle, we adopt the penalty method like TrajOpt and propose the  $\mathcal{L}$ -restart method based on AGD. Its numerical MAP only requires the first order momenta to reduce memory resources consumed for the LM-Hessian of GPMP. Moreover, it adopts AGD to generalize the leapfrog method adopted by CHOMP and reestimates the Lipschitz constant to elevate the convergence rate.

STOMP proposes a stochastic trajectory optimization to save the computation resource for gradient (i.e., momentum) estimation and overcome the local minima of some nonconvex cases. However, its small covariance ensuring the safe descent restrains the search space. Our method proposes ASTO on STOMP to gather the environmental information of the objective functional. To enlarge the searching space, ASTO samples trajectory obeying the Gaussian distribution (with a significant covariance) even the uniform distribution. Moreover, it adopts EM for reward and proposes the AMA method to reward the policy learning of the GP model.

To find the Hamiltonian minimum, CHOMP adopts HMC, which alternates between the leapfrog and Monte-Carlo methods. However, AGP-STO first proposes *MinAprch* to judge the local minima approaching when reestimating the Lipschitz constant. It then learns the GP-policy via ASTO when the minimum approaches and performs a numerical MAP of the

learned policy. Moreover, we upgrade AGP-STO to iAGP-STO, which selects the guidance waypoints and optimizes the sub-trajectory incrementally to improve the success rate and computation efficiency, unlike iGPMP upgrade, directly applying iSAM2 to GPMP.

## XII. CONCLUSION

iAGP-STO integrates a numerical and sampling method for optimal motion planning to overcome the local minima and converge to global minimum rapidly.

(i) The  $\mathcal{L}$ -reAGD method reestimates the Lipschitz constant to converge 95% faster in the semi-convex subspace.

(ii) The introduction of *MinAprch* judgment and ASTO helps search for the convex neighborhood of global minimum. It improves the success rate by 200% compared to the numerical methods and reduces the computation time by 65%-85% compared to the sampling method.

(iii) Furthermore, we use the incremental method based on Bayesian inference to optimize the whole trajectory via solving the noisy subproblems, which could expedite the whole trajectory optimization process by 25%- 50% and improve the success rate by 5% with searching space reduction.

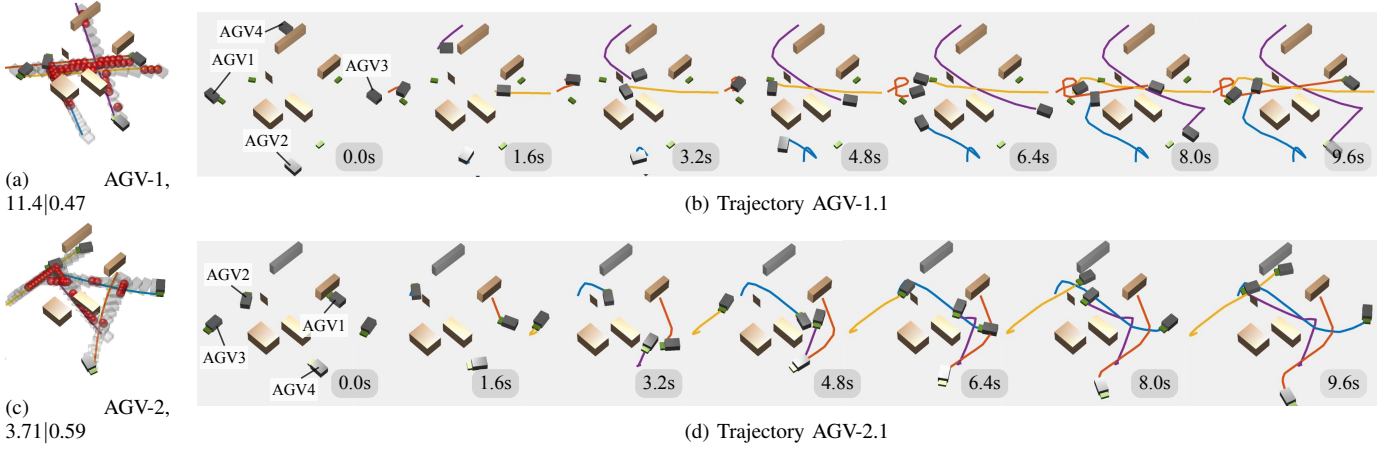


Fig. 12: A figure shows the results of multi-AGV allocation planned by iAGP-STO.

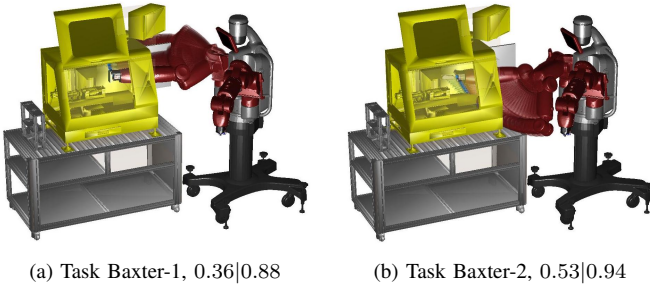


Fig. 13: Planning problems of rethink-Baxter assistance.

#### APPENDIX A PARAMETER DERIVATION OF AGD

According to Corollary 1 and Lemma 1, we can get

$$\Gamma_k = \frac{2}{k(k+1)}, \quad \sum_{\tau=k}^{N_{ag}} \Gamma_{\tau} = 2 \left( \frac{1}{k} - \frac{1}{N_{ag}} \right). \quad (50)$$

In this way, (4) can be scaled as

$$\begin{aligned} C_k &= 1 - \mathcal{L}_{\mathcal{F}} \lambda_k - \frac{\mathcal{L}_{\mathcal{F}} (\lambda_k - \beta_k)^2}{2\alpha_k \Gamma_k \lambda_k} \sum_{k=1}^{N_{ag}} \Gamma_{\tau} \\ &\geq 1 - \mathcal{L}_{\mathcal{F}} (1 + \vartheta_2 \alpha_k) \beta_k - \frac{\mathcal{L}_{\mathcal{F}} (\vartheta_2 \alpha_k \beta_k)^2}{2\alpha_k \Gamma_k \beta_k} \cdot \frac{2}{k} \\ &= 1 - \frac{1 + \vartheta_2 \alpha_k}{\vartheta_1} - \frac{\alpha_k \vartheta_2^2}{k \Gamma_k \vartheta_1} \geq \frac{-\vartheta_2^2 - \vartheta_2 + \vartheta_1 - 1}{\vartheta_1} \end{aligned} \quad (51)$$

when assigning  $\{\mathcal{F}, \mathcal{L}_{\mathcal{F}}\}$  to  $\{\Psi, \mathcal{L}_{\Psi}\}$ . So the condition

$$-\vartheta_2^2 - \vartheta_2 + \vartheta_1 - 1 > 0, \quad (52)$$

satisfies the prerequisite that  $C_k > 0, \vartheta_1 \geq 1, \vartheta_2 > 0$ . By the substitution from (51) into (5), we gain

$$\min_{k=1 \dots N_{ag}} \|\bar{\nabla} \mathcal{F}_k^{md}\|^2 \leq \frac{\vartheta_1^2 \mathcal{L}_{\mathcal{F}} (\mathcal{F}_0 - \mathcal{F}^*)}{N_{ag} (-\vartheta_2^2 - \vartheta_2 + \vartheta_1 - 1)}. \quad (53)$$

#### APPENDIX B DERIVATION OF ADAPTIVE STOCHASTIC

#### TRAJECTORY OPTIMIZATION

According to the definition of the reward  $\mathcal{R}$  in (34), we gain

$$\begin{aligned} \mathcal{R}(\mu', \mathcal{K}' | \mu, \mathcal{K}) &= \mathbb{E}_{\mathcal{F}_{M^*} | \Theta_{M^*}; \mu, \mathcal{K}} \log L(\mu', \mathcal{K}' | \theta_m, \mathcal{F}_m) \\ &= \sum_{m=1}^{M^*} p_m \left[ \log p_m - \frac{d \log 2\pi + \log |\mathcal{K}'| + \|\theta_m - \mu'\|_{\mathcal{K}'}^2}{2} \right] \end{aligned} \quad (54)$$

Then we could find the optimal policy via

$$\hat{\mu}, \hat{\mathcal{K}} = \underset{\mu', \mathcal{K}'}{\operatorname{argmin}} \mathcal{R}(\mu', \mathcal{K}' | \mu, \mathcal{K}) \quad (55)$$

informed by  $\Theta_{M^*}$ , which could be simplified as

$$\hat{\mu} = \underset{\mu'}{\operatorname{argmin}} \sum_{m=1}^{M^*} \frac{p_m}{2} \|\theta_m - \mu'\|_{\mathcal{K}'}^2 \Leftrightarrow \sum_{m=1}^{M^*} p_m (\theta_m - \mu') = 0, \quad (56)$$

$$\begin{aligned} \hat{\mathcal{K}} &= \underset{\mathcal{K}'}{\operatorname{argmin}} \sum_{k=1}^{M^*} \frac{p_m}{2} (\log |\mathcal{K}'| + \|\theta_m - \hat{\mu}\|_{\mathcal{K}'}^2) \\ &\Leftrightarrow \sum_{m=1}^{M^*} p_m [\mathcal{K}'^{-1} - \mathcal{K}'^{-1} (\theta_m - \mu')^{\otimes 2} \mathcal{K}'^{-1}] = 0, \end{aligned} \quad (57)$$

In this way, we gain the optimal policy

$$\hat{\mu} = \frac{\sum_{m=1}^{M^*} p_m \theta_m}{\sum_{m=1}^{M^*} p_m}, \quad \hat{\mathcal{K}} = \frac{\sum_{m=1}^{M^*} p_m (\theta_m - \hat{\mu})^{\otimes 2}}{\sum_{m=1}^{M^*} p_m}. \quad (58)$$

#### APPENDIX C DERIVATION OF ACCELERATED MOVING AVERAGING

According to Algorithm 3, we gain

$$\begin{aligned} \mu_{n+1}^{md} &= (1 - \alpha_n^{\mu})(\mu_n^{md} + \beta_n^{\mu} \nabla \hat{\mathcal{R}}_n^{md}) + \alpha_n^{\mu} (\mu_{n-1} + \lambda_n^{\mu} \nabla \hat{\mathcal{R}}_n^{md}) \\ &= \mu_n^{md} + [\beta_n^{\mu} + \alpha_n^{\mu} (\lambda_n^{\mu} - \beta_n^{\mu})] (\hat{\mu}_n - \mu_n^{md}) + \alpha_n^{\mu} (\mu_{n-1} - \mu_n^{md}) \end{aligned} \quad (59)$$

$$\mathcal{K}_{n+1}^{md} = \mathcal{K}_n^{md} + [\beta_n^{\kappa} + \alpha_n^{\kappa} (\lambda_n^{\kappa} - \beta_n^{\kappa})] (\hat{\mathcal{K}}_n - \mathcal{K}_n^{md}) + \alpha_n^{\kappa} (\mathcal{K}_{n-1} - \mathcal{K}_n^{md}) \quad (60)$$

Since  $\mu_n = \mu_{n-1} + \lambda_n^{\mu} (\hat{\mu}_n - \mu_n^{md})$  and  $\mu_0 = \mu_1^{md}$ , we get

$$\begin{aligned} \mu_{n-1} - \mu_n^{md} &= (1 - \alpha_{n-1}^{\mu}) [\mu_{n-2} - \mu_{n-1}^{md} \\ &\quad + (\lambda_{n-1}^{\mu} - \beta_{n-1}^{\mu}) (\hat{\mu}_{n-1} - \mu_{n-1}^{md})] \\ &= \sum_{i=1}^{n-1} \prod_{j=i}^{n-1} (1 - \alpha_j^{\mu}) (\lambda_i^{\mu} - \beta_i^{\mu}) (\hat{\mu}_i - \mu_i^{md}), \end{aligned} \quad (61)$$

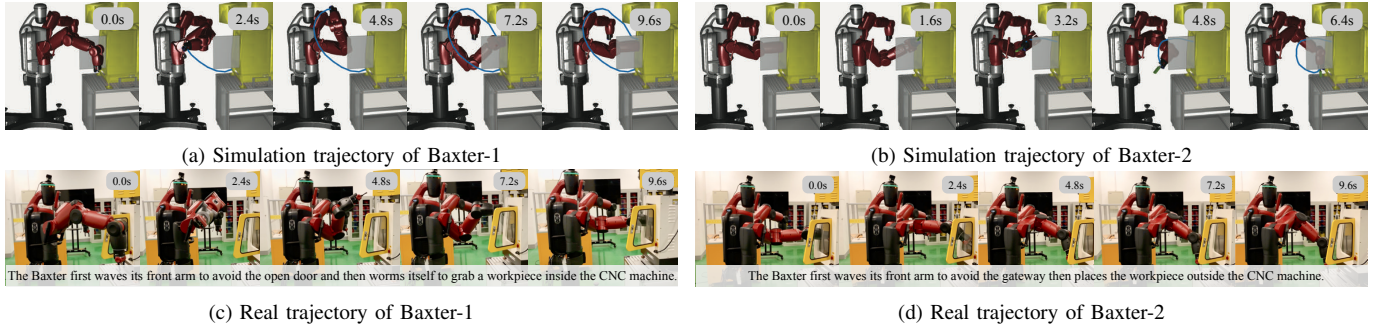


Fig. 14: A figure shows the results of rethink-Baxter assistance planned by iAGP-STO.

$$\mathcal{K}_{n-1} - \mathcal{K}_n^{md} = \sum_{i=1}^{n-1} \prod_{j=i}^{n-1} (1 - \alpha_j^\kappa) (\lambda_i^\kappa - \beta_i^\kappa) (\hat{\mathcal{K}}_i - \mathcal{K}_i^{md}), \quad (62)$$

then substitute (61) into (59) and substitute (62) into (60) to gain the AMA method:

$$\begin{aligned} \mu_{n+1}^{md} &= \mu_n^{md} + \alpha_n (\lambda_n - \beta) (\hat{\mu}_n - \mu_n^{md}) \\ &\quad + \alpha_{n-1} \Gamma_{n-1} \sum_{i=1}^{n-1} \Gamma_{i-1}^{-1} (\lambda_i - \beta) (\hat{\mu}_i - \mu_i^{md}), \\ \mathcal{K}_{n+1}^{md} &= \mathcal{K}_n^{md} + \alpha_n (\lambda_n - \beta) (\hat{\mathcal{K}}_n - \mathcal{K}_n^{md}) \\ &\quad + \alpha_{n-1} \Gamma_{n-1} \sum_{i=1}^{n-1} \Gamma_{i-1}^{-1} (\lambda_i - \beta) (\hat{\mathcal{K}}_i - \mathcal{K}_i^{md}). \end{aligned} \quad (63)$$

So when we set  $\beta_n^\mu = (1 - \alpha^\mu)^n$ ,  $\beta_n^\kappa = (1 - \alpha^\kappa)^n$  and  $\lambda_n^\mu = 1 + \beta_n^\mu$ ,  $\lambda_n^\kappa = 1 + \beta_n^\kappa$ , we gain the qAdam method:

$$\begin{aligned} \mu_{n+1}^{md} &= \mu_n^{md} + [(1 - \alpha^\mu)^n + \alpha^\mu] (\hat{\mu}_n - \mu_n^{md}) \\ &\quad + \alpha^\mu \sum_{i=1}^{n-1} \prod_{j=i}^{n-1} (1 - \alpha^\mu) (\hat{\mu}_i - \mu_i^{md}) \\ &= \hat{\mu}_n - \alpha^\mu \frac{(1 - \alpha^\mu)(1 - (1 - \alpha^\mu)^{n-1})}{1 - (1 - \alpha^\mu)} (\hat{\mu}_n - \mu_n^{md}) \\ &\quad + \alpha^\mu \sum_{i=1}^{n-1} \prod_{j=i}^{n-1} (1 - \alpha^\mu) (\hat{\mu}_i - \mu_i^{md}) \\ &= \hat{\mu}_n + \alpha^\mu \sum_{i=1}^{n-1} \frac{(\hat{\mu}_i - \mu_i^{md}) - (\hat{\mu}_n - \mu_n^{md})}{(1 - \alpha^\mu)^{i-n}}, \\ \mathcal{K}_{n+1}^{md} &= \hat{\mathcal{K}}_n + \alpha^\kappa \sum_{i=1}^{n-1} \frac{(\hat{\mathcal{K}}_i - \mathcal{K}_i^{md}) - (\hat{\mathcal{K}}_n - \mathcal{K}_n^{md})}{(1 - \alpha^\kappa)^{i-n}}. \end{aligned} \quad (64)$$

$$\mathcal{K}_{n+1}^{md} = \hat{\mathcal{K}}_n + \alpha^\kappa \sum_{i=1}^{n-1} \frac{(\hat{\mathcal{K}}_i - \mathcal{K}_i^{md}) - (\hat{\mathcal{K}}_n - \mathcal{K}_n^{md})}{(1 - \alpha^\kappa)^{i-n}}. \quad (65)$$

#### ACKNOWLEDGMENT

The work of this paper is partially supported by the National Natural Science Foundation of China (No. 52175032), the Key R&D Program of Zhejiang Province (2020C01025, 2020C01026), and Robotics Institute of Zhejiang University Grant (K11808).

#### REFERENCES

- [1] M. Zucker, N. Ratliff, A. D. Dragan, M. Pivtoraiko, M. Klingensmith, C. M. Dellin, J. A. Bagnell, and S. S. Srinivasa, "Chomp: Covariant hamiltonian optimization for motion planning," *The International Journal of Robotics Research*, vol. 32, no. 9-10, pp. 1164-1193, 2013.
- [2] J. Schulman, Y. Duan, J. Ho, A. Lee, I. Awwal, H. Bradlow, J. Pan, S. Patil, K. Goldberg, and P. Abbeel, "Motion planning with sequential convex optimization and convex collision checking," *The International Journal of Robotics Research*, vol. 33, no. 9, pp. 1251-1270, 2020/03/01 2014.
- [3] M. Mukadam, J. Dong, X. Yan, F. Dellaert, and B. Boots, "Continuous-time gaussian process motion planning via probabilistic inference," *The International Journal of Robotics Research*, vol. 37, no. 11, pp. 1319-1340, 2018.
- [4] S. M. LaValle *et al.*, "Rapidly-exploring random trees: A new tool for path planning," 1998.
- [5] J. J. Kuffner and S. M. LaValle, "Rrt-connect: An efficient approach to single-query path planning," in *Proceedings 2000 ICRA. Millennium Conference. IEEE International Conference on Robotics and Automation. Symposia Proceedings (Cat. No.00CH37065)*, vol. 2, April 2000, pp. 995-1001 vol.2.
- [6] S. Karaman and E. Frazzoli, "Sampling-based algorithms for optimal motion planning," *The international journal of robotics research*, vol. 30, no. 7, pp. 846-894, 2011.
- [7] M. Kalakrishnan, S. Chitta, E. Theodorou, P. Pastor, and S. Schaal, "Stomp: Stochastic trajectory optimization for motion planning," in *2011 IEEE International Conference on Robotics and Automation*, May 2011, pp. 4569-4574.
- [8] L. Kavraki and J.-C. Latombe, "Randomized preprocessing of configuration for fast path planning," in *Proceedings of the 1994 IEEE International Conference on Robotics and Automation*. IEEE, 1994, pp. 2138-2145.
- [9] D. Berenson, S. Srinivasa, and J. Kuffner, "Task space regions: A framework for pose-constrained manipulation planning," *The International Journal of Robotics Research*, vol. 30, no. 12, pp. 1435-1460, 2011.
- [10] T. Stouraitis, I. Chatzinikolaïdis, M. Gienger, and S. Vijayakumar, "Online hybrid motion planning for dyadic collaborative manipulation via bilevel optimization," *IEEE Transactions on Robotics*, vol. 36, no. 5, pp. 1452-1471, 2020.
- [11] S. Ghadimi and G. Lan, "Accelerated gradient methods for nonconvex nonlinear and stochastic programming," *Mathematical Programming*, vol. 156, no. 1-2, pp. 59-99, 2016.
- [12] J. Nocedal and S. Wright, *Numerical optimization*. Springer Science & Business Media, 2006.
- [13] J. Schulman, J. Ho, A. X. Lee, I. Awwal, H. Bradlow, and P. Abbeel, "Finding locally optimal, collision-free trajectories with sequential convex optimization," in *Robotics: science and systems*, vol. 9, no. 1. Citeseer, 2013, pp. 1-10.
- [14] C. Park, J. Pan, and D. Manocha, "Itomp: Incremental trajectory optimization for real-time replanning in dynamic environments," in *Proceedings of the Twenty-Second International Conference on International Conference on Automated Planning and Scheduling*, ser. ICAPS'12. AAAI Press, 2012, pp. 207-215.
- [15] S. Quinlan and O. Khatib, "Elastic bands: connecting path planning and control," in *[1993] Proceedings IEEE International Conference on Robotics and Automation*, May 1993, pp. 802-807 vol.2.
- [16] S. Quinlan, "Real-time modification of collision-free paths," Ph.D. dissertation, Stanford University, Stanford, CA, USA, 1995.
- [17] S. Osher and R. Fedkiw, *Signed Distance Functions*. New York, NY: Springer New York, 2003, pp. 17-22.
- [18] C. Liu and M. Tomizuka, "Algorithmic safety measures for intelligent industrial co-robots," in *2016 IEEE International Conference on Robotics and Automation (ICRA)*, May 2016, pp. 3095-3102.
- [19] J. Dong, M. Mukadam, F. Dellaert, and B. Boots, "Motion planning as probabilistic inference using gaussian processes and factor graphs," in *Robotics: Science and Systems*, vol. 12, 2016, p. 4.
- [20] M. Kaess, H. Johannsson, R. Roberts, V. Ila, J. J. Leonard, and F. Dellaert, "isam2: Incremental smoothing and mapping using the bayes

- tree,” *The International Journal of Robotics Research*, vol. 31, no. 2, pp. 216–235, 2012.
- [21] M. Toussaint and C. Goerick, *A Bayesian View on Motor Control and Planning*. Berlin, Heidelberg: Springer Berlin Heidelberg, 2010, pp. 227–252.
- [22] L. Paull, M. Seto, and H. Li, “Area coverage planning that accounts for pose uncertainty with an auv seabed surveying application,” in *2014 IEEE International Conference on Robotics and Automation (ICRA)*, May 2014, pp. 6592–6599.
- [23] L. Paull, M. Seto, J. J. Leonard, and H. Li, “Probabilistic cooperative mobile robot area coverage and its application to autonomous seabed mapping,” *The International Journal of Robotics Research*, vol. 37, no. 1, pp. 21–45, 2018.
- [24] A. Kapoor, K. Grauman, R. Urtasun, and T. Darrell, “Gaussian processes for object categorization,” *International Journal of Computer Vision*, vol. 88, no. 2, pp. 169–188, 2010.
- [25] E. Rodner, A. Freytag, P. Bodesheim, B. Fröhlich, and J. Denzler, “Large-scale gaussian process inference with generalized histogram intersection kernels for visual recognition tasks,” *International Journal of Computer Vision*, vol. 121, no. 2, pp. 253–280, 2017.
- [26] E. Huang, M. Mukadam, Z. Liu, and B. Boots, “Motion planning with graph-based trajectories and gaussian process inference,” in *2017 IEEE International Conference on Robotics and Automation (ICRA)*, May 2017, pp. 5591–5598.
- [27] K. Levenberg, “A method for the solution of certain non-linear problems in least squares,” *Quarterly of Applied Mathematics*, vol. 2, no. 2, pp. 164–168, 1944.
- [28] T. Sugihara, “Solvability-unconcerned inverse kinematics by the levenberg-marquardt method,” *IEEE Transactions on Robotics*, vol. 27, no. 5, pp. 984–991, Oct 2011.
- [29] H. Badreddine, S. Vandewalle, and J. Meyers, “Sequential quadratic programming (sqp) for optimal control in direct numerical simulation of turbulent flow,” *Journal of Computational Physics*, vol. 256, pp. 1–16, 2014.
- [30] F. E. Curtis, T. Mitchell, and M. L. Overton, “A bfgs-sqp method for nonsmooth, nonconvex, constrained optimization and its evaluation using relative minimization profiles,” *Optimization Methods and Software*, vol. 32, pp. 148–181, 2017.
- [31] J. Lo, G. Huang, and D. Metaxas, “Human motion planning based on recursive dynamics and optimal control techniques,” *Multibody System Dynamics*, vol. 8, no. 4, pp. 433–458, 2002.
- [32] D. C. Liu and J. Nocedal, “On the limited memory bfgs method for large scale optimization,” *Mathematical programming*, vol. 45, no. 1-3, pp. 503–528, 1989.
- [33] C. Zhu, R. H. Byrd, P. Lu, and J. Nocedal, “Algorithm 778: L-bfgs-b: Fortran subroutines for large-scale bound-constrained optimization,” *ACM Transactions on Mathematical Software (TOMS)*, vol. 23, no. 4, pp. 550–560, 1997.
- [34] M. Al-baali, “Descent property and global convergence of the fletcher-reeves method with inexact line search,” *IMA Journal of Numerical Analysis*, vol. 5, no. 1, pp. 121–124, Jan. 1985.
- [35] A. R. Conn, N. I. M. Gould, and P. L. Toint, *Trust-Region Methods*. USA: Society for Industrial and Applied Mathematics, 2000.
- [36] J. Schulman, S. Levine, P. Abbeel, M. Jordan, and P. Moritz, “Trust region policy optimization,” in *International conference on machine learning*, 2015, pp. 1889–1897.
- [37] L. Bottou, *On-line Learning and Stochastic Approximations*, ser. Publications of the Newton Institute. Cambridge University Press, 1999, pp. 9–42.
- [38] D. P. Kingma and J. Ba, “Adam: A method for stochastic optimization,” *arXiv preprint arXiv:1412.6980*, 2014.
- [39] G. Hinton, S. Nitish, and S. Kevin, “Neural networks for machine learning lecture 6a overview of mini-batch gradient descent,” Department of Computer Science, University of Toronto, Tech. Rep. 14, 02 2012.
- [40] J. Duchi, E. Hazan, and Y. Singer, “Adaptive subgradient methods for online learning and stochastic optimization,” *J. Mach. Learn. Res.*, vol. 12, pp. 2121–2159, Jul. 2011.
- [41] Y. Feng, H. Zhang, J. Wang, and G. Lu, “Incrementally stochastic and accelerated gradient information mixed optimization for manipulator motion planning,” *arXiv preprint arXiv:2108.09490*, 2021.
- [42] Y. Nesterov, “A method for unconstrained convex minimization problem with the rate of convergence  $O(1/k^2)$ ,” in *Doklady an ussr*, vol. 269, 1983, pp. 543–547.
- [43] S. Ji and J. Ye, “An accelerated gradient method for trace norm minimization,” in *Proceedings of the 26th Annual International Conference on Machine Learning*, ser. ICML ’09. New York, NY, USA: Association for Computing Machinery, 2009, pp. 457–464.
- [44] C. Hu, W. Pan, and J. T. Kwok, “Accelerated gradient methods for stochastic optimization and online learning,” in *Advances in Neural Information Processing Systems 22*, Y. Bengio, D. Schuurmans, J. D. Lafferty, C. K. I. Williams, and A. Culotta, Eds. Curran Associates, Inc., 2009, pp. 781–789.
- [45] C. Jin, P. Netrapalli, and M. I. Jordan, “Accelerated gradient descent escapes saddle points faster than gradient descent,” 2017.
- [46] P. E. Hart, N. J. Nilsson, and B. Raphael, “A formal basis for the heuristic determination of minimum cost paths,” *IEEE Transactions on Systems Science and Cybernetics*, vol. 4, no. 2, pp. 100–107, July 1968.
- [47] A. R. Wade, “Explicit laws of large numbers for random nearest-neighbour-type graphs,” *Advances in Applied Probability*, vol. 39, no. 2, pp. 326–342, 2007.
- [48] A. Perez, R. Platt, G. Konidaris, L. Kaelbling, and T. Lozano-Perez, “Lqr-rrt\*: Optimal sampling-based motion planning with automatically derived extension heuristics,” in *2012 IEEE International Conference on Robotics and Automation*, May 2012, pp. 2537–2542.
- [49] L. E. Kavraki, P. Svestka, J. . Latombe, and M. H. Overmars, “Probabilistic roadmaps for path planning in high-dimensional configuration spaces,” *IEEE Transactions on Robotics and Automation*, vol. 12, no. 4, pp. 566–580, Aug 1996.
- [50] L. E. Kavraki, M. N. Kolountzakis, and J. . Latombe, “Analysis of probabilistic roadmaps for path planning,” *IEEE Transactions on Robotics and Automation*, vol. 14, no. 1, pp. 166–171, Feb 1998.
- [51] C. R. Garrett, T. Lozano-Pérez, and L. P. Kaelbling, “Ffrob: Leveraging symbolic planning for efficient task and motion planning,” *The International Journal of Robotics Research*, vol. 37, no. 1, pp. 104–136, 2018.
- [52] L. Petrović, J. Peršić, M. Seder, and I. Marković, “Stochastic optimization for trajectory planning with heteroscedastic gaussian processes,” in *2019 European Conference on Mobile Robots (ECMR)*, 2019, pp. 1–6.
- [53] T. Osa, “Multimodal trajectory optimization for motion planning,” *The International Journal of Robotics Research*, vol. 39, no. 8, pp. 983–1001, 2020.
- [54] P. Armand and R. Omhenni, “A globally and quadratically convergent primal–dual augmented lagrangian algorithm for equality constrained optimization,” *Optimization Methods and Software*, vol. 32, no. 1, pp. 1–21, 2017.
- [55] P. Srivastava and J. Cortés, “Nesterov acceleration for equality-constrained convex optimization via continuously differentiable penalty functions,” *IEEE Control Systems Letters*, vol. 5, no. 2, pp. 415–420, 2021.
- [56] Z.-J. Shi and J. Shen, “New inexact line search method for unconstrained optimization,” *Journal of optimization theory and applications*, vol. 127, no. 2, pp. 425–446, 2005.
- [57] I. Loshchilov and F. Hutter, “Sgdr: Stochastic gradient descent with warm restarts,” *arXiv preprint arXiv:1608.03983*, 2016.
- [58] B. O’Donoghue and E. Candès, “Adaptive restart for accelerated gradient schemes,” *Foundations of Computational Mathematics*, vol. 15, no. 3, pp. 715–732, 2015.
- [59] J. Liu, L. Yuan, and J. Ye, “An efficient algorithm for a class of fused lasso problems,” in *Proceedings of the 16th ACM SIGKDD International Conference on Knowledge Discovery and Data Mining*, ser. KDD ’10. New York, NY, USA: Association for Computing Machinery, 2010, pp. 323–332.
- [60] C. F. J. Wu, “On the convergence properties of the em algorithm,” *Ann. Statist.*, vol. 11, no. 1, pp. 95–103, 03 1983.
- [61] X. Jiang, B. Dong, L. Xie, and L. Sweeney, “Adaptive gaussian process for short-term wind speed forecasting,” in *Proceedings of the 2010 Conference on ECAI 2010: 19th European Conference on Artificial Intelligence*. NLD: IOS Press, 2010, pp. 661–666.
- [62] P. Dayan and G. E. Hinton, “Using Expectation-Maximization for Reinforcement Learning,” *Neural Computation*, vol. 9, no. 2, pp. 271–278, 02 1997.
- [63] A. Kanazawa, J. Kinugawa, and K. Kosuge, “Adaptive motion planning for a collaborative robot based on prediction uncertainty to enhance human safety and work efficiency,” *IEEE Transactions on Robotics*, vol. 35, no. 4, pp. 817–832, 2019.
- [64] A. KANAZAWA, J. KINUGAWA, and K. KOSUGE, “Incremental learning of spatial-temporal features in human motion patterns with mixture model for planning motion of a collaborative robot in assembly lines,” in *2019 International Conference on Robotics and Automation (ICRA)*, 2019, pp. 7858–7864.
- [65] F. Dellaert, “Factor graphs and gtsam: A hands-on introduction,” Georgia Institute of Technology, Tech. Rep., 2012.
- [66] N. Ratliff, M. Zucker, J. A. Bagnell, and S. Srinivasa, “Chomp: Gradient optimization techniques for efficient motion planning,” in *2009 IEEE*

*International Conference on Robotics and Automation*, May 2009, pp. 489–494.